Mathematical Relationships between Spinal Motoneuron Properties

Arnault Caillet[1], Andrew T.M. Phillips[1], Dario Farina[2,*], Luca Modenese[1,*]

[1]Department of Civil and Environmental Engineering, Imperial College London, SW7 2AZ, UK
[2]Department of Bioengineering, Imperial College London, SW7 2AZ, UK
Email: arnault.caillet17@imperial.ac.uk

* These authors have equal contributions and share the senior authorship

NUMBER OF PAGES: 43

NUMBER OF FIGURES: 7

NUMBER OF TABLES: 8

NUMBER OF WORDS FOR ABSTRACT: 194

CONFLICT OF INTEREST STATEMENT: The authors declare no competing financial interests.

ACKNOWLEDGEMENTS: Imperial College Skempton Scholarship to A.C. and Imperial College Research Fellowship to L.M.

Abstract

Our understanding of the behaviour of alpha-motoneurons (MNs) in mammals partly relies on our knowledge of the relationships between MN membrane properties, such as MN size, resistance, rheobase, capacitance, time constant, axonal conduction velocity and afterhyperpolarization period. Based on scattered but converging evidence, current experimental studies and review papers qualitatively assumed that some of these MN properties are related. In this systematic meta-analysis, we reprocessed the data from 40 experimental studies in adult cat, rat and mouse MN preparations *in vivo* to empirically derive mathematical relations between experimentally measured MN electrophysiological and anatomical properties. These mathematical relationships provide the first validated framework of MN-specific morphometric and electrophysiological properties that reproduce published experimental mammal data *in vivo*. These relationships moreover support the classic description of a MN as a membrane equivalent electrical circuit and describe for the first time the association between MN size and MN membrane capacitance and time constant. The obtained relationships finally indicate that motor units are recruited in order of increasing MN size, muscle unit size, MN rheobase, unit force recruitment thresholds and tetanic forces, but underlines that MN size and recruitment order may not be related to motor unit type.

Keywords: motor neuron, motoneuron, motor neuron size, mathematical relationships, motor unit, Henneman's size principle

Introduction

Our understanding of the behaviour of alpha-motoneurons (MNs) in mammals partly relies on the knowledge of the relationships between the MN morphometric and electrophysiological properties reported in Table 1. Direct measurement of some of these properties has been performed in animal studies and yielded some significant correlations, such as the MN input resistance being strongly inversely associated to rheobase current (Krawitz et al., 2001; Button et al., 2008; Krutki et al., 2015; Huh et al., 2021). Further investigating such associations in mammals is important to improve both our understanding of MN pool behaviour and the computational models of MNs. Indeed, due to the current lack of mathematical descriptions of the relationships between MN morphometric and/or electrophysiological quantities, MN property profiles in computational models are typically built with scattered data from a relatively small number of experimental studies. Such generic MN profiles indicate reasonable orders of magnitude but result in a lack of inter-consistency between the MN properties. This approach yields obvious limitations when the sets of physiological and MN-specific characteristics must be known, as in numerical models of a MN membrane equivalent electrical circuit (Izhikevich, 2004; Dong et al., 2011; Negro et al., 2016; Teeter et al., 2018).

To tackle these current limitations in our understanding of the working principles of MNs and in MN modelling, algebraic relationships must be derived between the main MN properties listed in Table 1. This could be done by concurrently measuring all properties in single MNs. However, because of technical difficulties in measuring MN morphometric and electrophysiological properties *in vivo*, it is currently challenging to experimentally measure a complete and reliable set of MN-specific properties for a large sample of MNs. Specialised experimental set-ups could measure a maximum of six MN properties concurrently in animal preparations, and for limited numbers of MNs (Gustafsson & Pinter, 1984a; Gustafsson & Pinter, 1984b).

Our knowledge of MN properties and their associations is therefore currently limited to a series of datasets that individually provide a crude picture of MN physiological and biophysical features but not a detailed understanding of the working principles of MNs. For this reason, the statements reported in review papers on the associations between MN properties rely on converging conclusions from independent studies and remain speculative (Henneman, 1981; Burke, 1981; Binder et al., 1996; Powers & Binder, 2001; Kernell, 2006; Heckman & Enoka, 2012). While qualitative associations, such as between MN size and resistance (Kernell & Zwaagstra, 1981; Burke et al., 1982), have led to extensions of Henneman's size principle (Henneman, 1957; Wuerker et al., 1965; Henneman et al., 1965a; Henneman et al., 1965b; Henneman et al., 1974; Henneman, 1981; Henneman, 1985), other relationships, such as between MN size and membrane capacitance or time constant, are not known.

Therefore, algebraic relationships between MN properties must be extrapolated from existing data, taking all data into account in a single mathematical framework.

Here, we derived and validated currently unknown mathematical relationships between any pair of the MN morphometric and electrophysiological cat properties listed in Table 1 by reprocessing and merging the published data from 18 available experimental studies in adult cat preparations *in vivo*. In this way, we first demonstrate that the electrophysiological properties reported in Table 1 are all associated to each other and can be precisely predicted by MN size in cats. We then assess whether the cat mathematical relationships apply to other mammals by validating them with data from 9 adult rat and mouse studies *in vivo*. These empirical relationships provide for the first time a mathematical framework for the association between any pair of spinal MN properties and for the derivation of MN profiles of MN-specific morphometric and electrophysiological properties that reproduce published experimental mammal data *in vivo*. Finally, using additional correlations obtained between some MN and muscle unit (mU) properties from 14 mammal studies, we discuss the empirical relationships obtained between MN properties in the context of Henneman's size principle.

Table 1. The motoneuron (MN) and muscle unit (mU) properties investigated in this study with their notations and SI base units. S_{MN} is the size of the MN. As reproduced in Table 2, the MN size S_{MN} is adequately described by measures of the MN surface area S_{neuron} and the soma diameter D_{soma}. R and R_m define the MN-specific electrical resistance properties of the MN and set the value of the MN-specific current threshold I_{th} (Binder et al., 1996; Powers & Binder, 2001; Heckman & Enoka, 2012). C and C_m (constant among the MN pool) define the capacitance properties of the MN and contribute to the definition of the MN membrane time constant τ (Gustafsson & Pinter, 1984b; Zengel et al., 1985). ΔV_{th} is the constant amplitude of the membrane voltage depolarization threshold relative to resting state required to elicit an action potential. I_{th} is the corresponding electrical current causing a membrane depolarization of ΔV_{th}. AHP is defined in most studies as the duration between the action potential onset and the time at which the MN membrane potential meets the resting state after being hyperpolarized. ACV is the axonal conduction velocity of the elicited action potentials on the MN membrane. S_{mU} is the size of the mU. As indicated in Table 2, the mU size S_{mU} is adequately described by measures of (1) the sum of the cross-sectional areas (CSAs) of the fibres composing the mU CSA^{tot}, (2) the mean fibre CSA CSA^{mean}, (3) the innervation ratio IR, i.e. the number of innervated fibres constituting the mU, and (4) the mU tetanic force F^{tet}. The muscle force at which a mU starts producing mU force is called mU force recruitment threshold F^{th}.

	Properties	**Notation**	**Unit**
Motoneuron (MN) properties	Size:	S_{MN}	
	Neuron surface area	S_{neuron}	$[m^2]$
	Soma diameter	D_{soma}	$[m]$
	Resistance	R	$[\Omega]$
	Specific resistance per unit area	R_m	$[\Omega \cdot m^2]$
	Capacitance	C	$[F]$
	Specific capacitance per unit area	C_m	$[F \cdot m^{-2}]$
	Time constant	τ	$[s]$
	Rheobase (current recruitment threshold)	I_{th}	$[A]$
	Voltage threshold	ΔV_{th}	$[V]$
	Afterhyperpolarization period	AHP	$[s]$
	Conduction velocity	ACV	$[m \cdot s^{-1}]$
Muscle unit (mU) properties	Size:	S_{mU}	
	Total fibre cross-sectional area (CSA)	CSA^{tot}	$[m^2]$
	Mean fibre CSA	CSA^{mean}	$[m^2]$
	Innervation ratio	IR	[ ]
	Tetanic force	F^{tet}	$[N]$
	Force recruitment threshold	F^{th}	$[N]$

Methods

Eligible studies

To optimize inter-study analysis, this meta-analysis focuses exclusively on studies, named "eligible" in the following, that concurrently measured at least two of the morphometric and/or electrophysiological properties reported in Table 1 in individual spinal alpha-motoneurons of healthy adult cats, rats and mice observed *in vivo*. Larval and postnatal specimens were therefore disregarded because of the pronounced age-related variance (Highlander et al., 2020) in the mean values of the electrophysiological properties listed in Table 1, which corroborates the non-extrapolability of neonatal neuronal circuitry to older ages (Song et al., 2006; Carp et al., 2008; Nakanishi & Whelan, 2010; Mitra & Brownstone, 2012). Due to the nonlinear inter-species scalability of the spinal alpha-MN electrophysiological and morphometric properties (Manuel et al., 2019) and a pronounced variance in the inter-species mean values (Highlander et al., 2020), non-mammalian species were disregarded, while the retained data from cats, rats and mice were processed separately. Highlander et al. (2020) also report an 'unexplained' variance in the mean property values reported between studies investigating specimens of the same species, sex and age, which may be explained by differences between *in vivo* and *in vitro* protocols (Carp et al., 2008). For this reason, only *in vivo* studies were considered in this meta-analysis, while most *in vitro* studies had already been disregarded at this stage as dominantly performed on neonatal specimens due to experimental constraints (Manuel et al., 2009a; Mitra & Brownstone, 2012).

To build an extensive set of eligible studies, the output of the systematic websearch provided in Highlander et al. (2020) was screened and used for a further search by reference lists. For convenience, in the following, the notation $\{A; B\}$ refers to the pair of morphometric or electrophysiological MN properties A and B, with $A, B \in \{S_{MN}; ACV; AHP; R; I_{th}; C;\ \tau\}$, defined in Table 1. The eligible studies generally provided clouds of data points for pairs $\{A; B\}$ of concurrently measured MN properties through scatter graphs. These plots were digitized using the online tool WebPlotDigitizer (Ankit, 2020). When an eligible study did not provide such processable data – most reported the mean $\pm SD$ property values of the cohort of measured MNs – the corresponding author was contacted to obtain the raw data of the measured MN properties, following approval of data sharing. Upon reception of data, datasets of all possible $\{A; B\}$ pairs were created and included into the metanalysis. As all but two eligible studies focused on lumbosacral MNs, the final set of eligible studies was constrained to MNs innervating hindlimb muscles to improve inter-study consistency.

From a preliminary screening of the retrieved studies, it was found that relatively more cat studies were obtained than rat and mouse studies, while the cat studies also investigated more $\{A; B\}$ pairs of morphometric and electrophysiological properties. The mathematical relationships sought in this paper between MN properties were thus derived from cat data, and the validated for extrapolation to rat and mouse data.

Relationships between MN properties

Normalized space

The sets of data retrieved from different cat studies for each property pair $\{A; B\}$ were merged into a 'global' dataset dedicated to that property pair. The $\{A; B\}$ data was also normalized for each study and transformed as a percentage of the maximum property value measured in the same study and normalized 'global' datasets were similarly created. A least squares linear regression analysis was performed for the $\ln(A) - \ln(B)$ transformation of each global dataset yielding relationships of the type $\ln(A) = a \cdot \ln(B) + k$, which were then converted into power relationships of the type $A = k \cdot B^a$ (eq.1). Power fitting was chosen for flexibility and simplicity. The adequacy of these global power trendlines and the statistical significance of the correlations were assessed with the coefficient of determination r^2 (squared value of the Pearson's correlation coefficient) and a threshold of 0.01 on the p-value of the regression analysis, respectively. For each $\{A; B\}$ pair, the normalized global datasets systematically returned both a higher r^2 and a lower p-value than the datasets of absolute $\{A; B\}$ values, in agreement with the 'unexplained' inter-experimental variance reported in (Highlander et al., 2020). It was therefore decided to investigate the $\{A; B\}$ pairs of MN properties in the normalized space using the normalized global datasets to improve the cross-study analysis.

Size-dependent normalized relationships

From inspection of the considered cat studies, most of the investigated MN property pairs comprised either a direct measurement of MN size, noted as S_{MN} in this study, or another variable strongly associated to size, such as axonal conduction velocity (ACV) or afterhyperpolarization period (AHP). Accordingly, and consistently with Henneman's size principle, we identified S_{MN} as the reference MN property with respect to which relationships with the electrophysiological MN properties in Table 1 were investigated.

To integrate the data from all global normalized datasets into the final relationships, the MN properties in Table 1 were processed in a step-by-step manner in the order $ACV, AHP, R, I_{th}, C, \tau$, as reproduced in Figure 1 for two arbitrary properties, to seek a 'final' power relationship of the type eq.1 between each of them and S_{MN}. For each electrophysiological property A and each $\{A; B\}$ dataset, we

considered two cases. If $B = S_{MN}$, the global dataset was not further processed as the electrophysiological property A was already related to MN size S_{MN} from experimental measurements. If $B \neq S_{MN}$, the global $\{A; B\}$ dataset was transformed into a new $\{A; S_{MN}\}$ dataset by converting the discrete values of B with the trendline regression $S_{MN} = k_d \cdot B^d$, which was obtained at a previous step of the data processing. With this dual approach, as many MN size-dependent $\{A; S_{MN}\}$ intermediary datasets as available $\{A; B\}$ global datasets were obtained for each property A. These size-dependent datasets were merged into a 'final' $\{A; S_{MN}\}$ dataset to which a least squares linear regression analysis was performed for the $\ln(A) - \ln(S_{MN})$ transformation, yielding relationships of the type $\ln(A) = c \cdot \ln(S_{MN}) + k$, which were converted into the power relationships:

$$A = k_c \cdot S_{MN}^c$$

The adequacy of these final power trendlines and the statistical significance of the correlations were assessed identically to the $\{A; B\}$ relationships derived directly from normalized experimental data, using the coefficient of determination r^2 (squared value of the Pearson's correlation coefficient) and a threshold of 0.01 on the p-value of the regression analysis, respectively. If $r^2 > 0.3$ (i.e. $r > 0.55$) and $p < 0.01$, another power trendline $S_{MN} = k_d \cdot A^d$ was fitted to the final dataset to describe the inverse relationship for $\{S_{MN}; A\}$ and used in the processing of the next-in-line property.

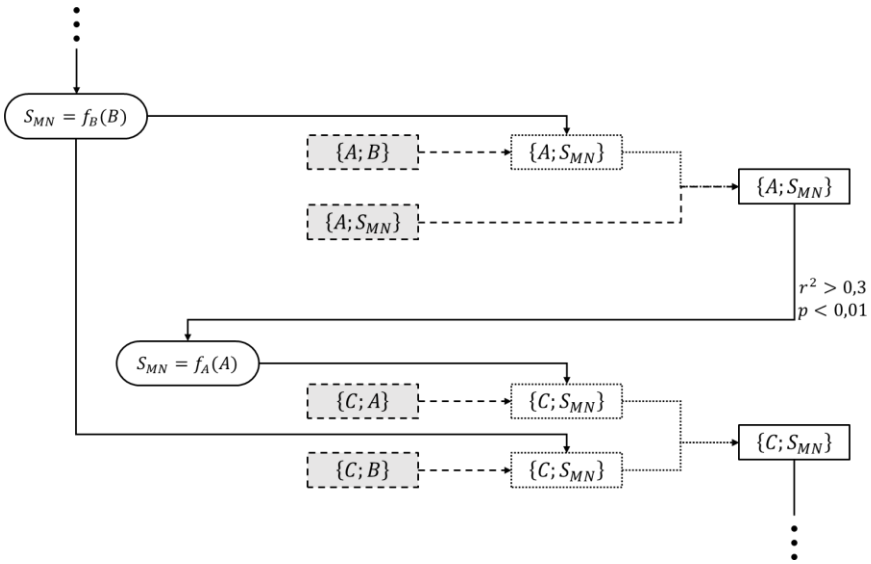

Figure 1. Two steps of the step-by-step approach to create the final MN size-related datasets. Here, the final $\{A; S_{MN}\}$ and $\{C; S_{MN}\}$ MN size-related datasets are created (right-side solid contour boxes), to which the final relationships $A, C = k_c \cdot S_{MN}^c$ were fitted. If $r^2 > 0.3$ and $p < 0.01$, power relationships $S_{MN} = f_A(A)$ and $S_{MN} = f_C(C)$ (oval boxes) were also fitted to the final $\{A; S_{MN}\}$ and $\{C; S_{MN}\}$ datasets. Here, $S_{MN} = f_B(B)$ was obtained from a previous unshown step. The normalized global datasets of experimental data (dashed-contour grey-filled boxes) were either directly included into the final datasets if already obtained as MN size-related, or first transformed into an MN size-related intermediary datasets (dotted-contour boxes) by converting the A and/or B properties into S_{MN} values with the $S_{MN} = f_A(A)$ and $S_{MN} = f_B(B)$ relationships. The final $\{A; S_{MN}\}$ and $\{C; S_{MN}\}$ MN size-related datasets were retained for further processing in this study.

Normalized mathematical relationships between electrophysiological properties

When a final relationship with S_{MN} was obtained for two MN properties A and B by the procedure described above, i.e., $A = k_{cA} \cdot S_{MN}^{c_A}$ and $B = k_{cB} \cdot S_{MN}^{c_B}$, one of the expressions was mathematically inverted and a third empirical relationship was derived for the property pair $\{A; B\}$:

$$A = \frac{k_{cA}}{(k_{cB})^{\frac{c_A}{c_B}}} \cdot (B)^{\frac{c_A}{c_B}} = k_e \cdot B^e$$

This procedure was applied to all possible $\{A; B\}$ pairs in Table 1.

Validation of the normalized relationships

The data in each $\{A; B\}$ global normalized dataset was initially randomized and therefore made independent from the studies constituting it. Each global dataset was then randomly split so that 70% of the data was processed to build the relationships, while the remaining 30% was used as a test dataset. The final size-related relationships $A = k_c \cdot S_{MN}^c$ and relationships between electrophysiological properties $A = k_e \cdot B^e$ were obtained as described previously using the 70%-datasets. These mathematical relationships were applied to the S_{MN} or B data in each 30%-dataset, yielding predicted values A. It was then assessed to what extent the mathematical relationships predicted the test data A by calculating the normalized maximum error (nME), the normalized root mean squared error ($nRMSE$) and the coefficient of determination r_{pred}^2 between predicted and control values of A in each 30%-dataset. This process was repeated for a total of 5 times, randomly creating novel 70-30 partitions of the global datasets. The nME, $nRMSE$ and r_{pred}^2 values were finally averaged across the five repetitions and the average r_{pred}^2 hence obtained was compared to the average of the r_{exp}^2 values obtained from the power trendlines least-squared fitted to the control data. This approach validated the relationships. Once validated with this cross-validation method, the final normalized size-dependent relationships $A = k_c \cdot S_{MN}^c$ and relationships between electrophysiological properties $A = k_e \cdot B^e$ were provided for the complete global datasets.

Scaling of the normalized relationships

The $A = k_c \cdot S_{MN}^c$ and $A = k_e \cdot B^e$ normalized relationships were finally scaled to typical cat property values in three steps. First, it was assessed from the literature the fold-range over which each MN property was to vary. S_{MN} varied over a q_S^E-fold range, taken as the average across cat studies of the ratios of minimum and maximum values measured for S_{MN}:

$$q_S^E = \frac{1}{N_{studies}} \sum_{i=1}^{N_{studies}} \left[\frac{(S_{MN_i})_{max}}{(S_{MN_i})_{min}} \right]$$

An experimental ratio q_A^E was similarly obtained for each electrophysiological property A. As $A = k_c \cdot S_{MN}^c$, any electrophysiological property A could theoretically vary over a $q_A^T = (q_S^E)^{|c|}$-fold range, which was compared to q_A^E for consistency in the results. Then, a theoretical range $[A_{min};\ A_{max}]$ of values were derived for each electrophysiological property A. Defining A_{min}^E and A_{max}^E as the respective average of the minimum and maximum A-values across studies, it was enforced $\frac{A_{max}}{A_{min}} = q_A^T$ and $\frac{A_{min}+A_{max}}{2} = \frac{A_{min}^E+A_{max}^E}{2}$ so that the $[A_{min};\ A_{max}]$ theoretical ranges were consistent with the normalized size-dependent relationships while best reproducing the experimental data from cat literature. A theoretical range for S_{MN} $[(S_{MN})_{min};\ (S_{MN})_{max}]$ was similarly built over the q_S^E-fold range previously derived. Finally, the intercept k_c in the size-dependent relationships $A = k_c \cdot S_{MN}^c$ was scaled as:

$$\begin{cases} k_c = \dfrac{A_{min}}{(S_{MN})_{min}^c} \ ; \ c > 0 \\ k_c = \dfrac{A_{max}}{(S_{MN})_{min}^c} \ ; \ c < 0 \end{cases}$$

A similar approach was used to mathematically derive the intercept k_e and scale the relationships $A = k_e \cdot B^e$ between electrophysiological properties.

Extrapolation to rats and mice

It was finally assessed whether the $A = k_c \cdot S_{MN}^c$ and $A = k_e \cdot B^e$ scaled relationships derived from cat data accurately predicted rat and mouse quantities reported in other experimental studies. These mathematical relationships were applied to the S_{MN} or B data in each $\{A; B\}$ global dataset of absolute values obtained for rats and mice independently. The accuracy in predicting the quantity A was assessed for each available dataset with the same three validation metrics used to validate the normalized power trend lines: the normalized maximum error (nME), the normalized root-mean-square error ($nRMSE$) and the coefficient of determination r^2 between predicted and experimental values of A.

Definitions of MN Size S_{MN} and mU size S_{mU}

MN Size S_{MN}

The eligible papers that performed both electrophysiological and morphometric measurements on the same MNs dominantly measured the MN soma diameter D_{soma} as an index of MN size. Therefore, we choose $S_{MN} = D_{soma}$ in the described methodology. In the literature on spinal MNs in adult mammals *in vivo*, the size of a MN S_{MN} is also related to the measures of the somal cross-sectional area CSA_{soma} (Gao et al., 2009; Friese et al., 2009; Deardorff et al., 2013; Mierzejewska-Krzyżowska et al., 2014;

Dukkipati et al., 2018), soma surface area S_{soma} (Ulfhake, B. & Kellerth, 1984; Brandenburg et al., 2020), axonal diameter D_{axon} (Cullheim, 1978), individual dendrite diameter $D_{dendrite}$ (Amendola & Durand, 2008; Carrascal et al., 2009; Mantilla et al., 2018), individual dendritic surface area $S_{dendrite}$ (Li et al., 2005; Obregón et al., 2009; Carrascal et al., 2009; Filipchuk & Durand, 2012; Kanjhan et al., 2015), total dendritic surface area (Ulfhake, Brun & Cullheim, 1988; Amendola & Durand, 2008; Brandenburg et al., 2020) or total MN surface area S_{neuron} (Burke et al., 1982) defined as the summed soma and dendritic surface areas.

In the references (Zwaagstra & Kernell, 1981; Ulfhake & Kellerth, 1981), a linear correlation between D_{soma} and the average diameter of the stem dendrites $D_{dendrite_{mean}}$ has been reported ($r > 0.62$, population size in $\{40; 82\}$ cells). Moreover, a linear or quasi-linear correlation has been found (Cullheim et al., 1987; Ulfhake, Brun & Cullheim, 1988; Moschovakis et al., 1991; Prakash et al., 2000; Li et al., 2005; Obregón et al., 2009; Mantilla et al., 2018) between the stem dendrite diameter $D_{dendrite}$ and the membrane surface area of the corresponding dendritic tree $S_{dendrite}$ ($r > 0.78$, population size in $[33; 342]$ dendrites). Therefore, from these studies, we can assume an approximate linear correlation between D_{soma} and the average dendritic surface area $S_{dendrite_{mean}}$. Moreover, the number of dendritic trees $N_{dendrites}$ per cell increases with increasing soma surface S_{soma} (Brandenburg et al., 2018), and a linear correlation between D_{soma} or $S_{dendrites}$ with $N_{dendrites}$ has been observed (Zwaagstra & Kernell, 1981; Ulfhake, Brun & Cullheim, 1988; Amendola & Durand, 2008) ($r > 0.40$, population size in $\{14; 32; 87\}$ cells). It was therefore assumed that D_{soma} and total dendritic surface area $S_{dendrite}^{tot}$ are linearly correlated. This assumption/approximation is consistent other conclusions of a linear correlations between D_{soma} and $S_{dendrite}^{tot}$ (Amendola & Durand, 2008; Brandenburg et al., 2020). Then, according to typical values of D_{soma}, S_{soma} and $S_{dendrites}^{tot}$ obtained from the studies previously cited, yielding $S_{dendrites}^{tot} \gg S_{soma}$, it was also assumed $S_{dendrites}^{tot} \approx S_{neuron}$. It is thus concluded that D_{soma} is linearly related to total neuron membrane area S_{neuron}, consistently with results by Burke et al. (1982) ($r = 0.61$, 57 cells).

For the above reasons and assumptions, the mathematical relationships $A = k_c \cdot S_{MN}^c$ derived previously, with $S_{MN} = D_{soma}$, were extrapolated with a gain to relationships between A and $S_{MN} = S_{neuron}$, notably permitting the definition of surface specific resistance R_m and capacitance C_m. Following the same method as described above, theoretical ranges $[(S_{neuron})_{min}; (S_{neuron})_{max}]$ were derived from additional morphometric studies on adult cat spinal alpha-motoneurons. The new relationships were extrapolated as $A = k_c \cdot D_{soma}^c = \frac{(S_{neuron})_{min}}{(D_{neuron})_{min}} \cdot S_{neuron}^c$.

It must however be highlighted that the conclusion of a linear correlation between D_{soma} and S_{neuron}, while plausible, is crude. Morphometric measurements of individual MNs are indeed difficult and

265 suffer many limitations. MN staining, slice preparations and MN reconstruction and identification are
266 complex experimental procedures requiring a large amount of work; the results from most of the cited
267 studies thus rely on relatively small pools of investigated MNs. Most cited studies did not account for
268 tissue shrinkage after dehydration, while some may have failed to assess the full dendritic trees from
269 MN staining techniques (Brandenburg et al., 2020), thus underestimating dendritic membrane
270 measurements. Moreover, before automated tools for image segmentation, landmark mapping and
271 surface tracking (Amendola & Durand, 2008; Obregón et al., 2009; Mierzejewska-Krzyżowska et al.,
272 2014) were available, morphometric measurements were performed from the manual reproduction
273 of the cell outline under microscope, yielding important operator errors reported to be of the order of
274 $\sim 0.5 \mu m$, i.e. $\sim 20\%$ stem diameter. In these studies, morphologic quantities were besides obtained
275 from geometrical approximations of the 2D MN shape, such as modelling the individual dendritic
276 branches as one (Cullheim et al., 1987) or more (Prakash et al., 2000) equivalent cylinders for the
277 derivation of $S_{dendrite}$. Morphometric measurement approaches also varied between studies; for
278 example, oval or circle shapes were best fitted by sight onto the soma outline and equivalent D_{soma}
279 quantities were derived either as the mean of measured maximum and minimum oval diameters or as
280 the equivalent diameter of the fitted circle. In these studies, CSA_{soma} and S_{soma} were therefore
281 derived by classical equations of circle and spheric surface areas, which contradicts the results by
282 Mierzejewska-Krzyżowska et al. (2014) obtained from surface segmentation of a linear relationship
283 between D_{soma} and CSA_{soma} ($r = 0.94$, 527 MNs). Finally, no correlation between soma size and
284 $N_{dendrites}$ was found (Ulfhake & Kellerth, 1981; Cullheim et al., 1987). Therefore, the linear correlation
285 between D_{soma} and S_{neuron} is plausible but crude and requires awareness of several important
286 experimental limitations and inaccuracies. Conclusions and predictions involving S_{neuron} should be
287 treated with care in this study as these morphometric measurements lack the precision of the
288 measures performed for the electrophysiological properties listed in Table 1.

289 Muscle unit size S_{mU}

290 To enable future comparisons between MN and mU properties, we here assess potential indices of the
291 mU size S_{mU} suggested in the literature. The size of a mU (S_{mU}) can be defined as the sum CSA^{tot} of
292 the cross-sectional areas CSAs of the innervated fibres composing the mU. CSA^{tot} depends on the mU
293 innervation ratio (IR) and on the mean CSA (CSA^{mean}) of the innervated fibres: $S_{mU} = CSA^{tot} = IR \cdot$
294 CSA^{mean}. CSA^{tot} was measured in a few studies on cat and rat muscles, either indirectly by
295 histochemical fibre profiling (Burke & Tsairis, 1973; Dum & Kennedy, 1980; Burke, 1981), or directly by
296 glycogen depletion, periodic acid Schiff (PAS) staining and fibre counting (Burke et al., 1982; Rafuse et
297 al., 1997). The mU tetanic force F^{tet} is however more commonly measured in animals. As the fibre
298 mean specific force σ is considered constant among the mUs of one muscle in animals (Lucas et al.,

1987; Enoka, 1995), the popular equation $F^{tet} = \sigma \cdot IR \cdot CSA^{mean}$ (Burke, 1981; Enoka, 1995) returns a linear correlation between F^{tet} and $IR \cdot CSA^{mean} = S_{mU}$ in mammals. Experimental results (Burke & Tsairis, 1973; Bodine et al., 1987; Chamberlain & Lewis, 1989; Kanda & Hashizume, 1992; Rafuse et al., 1997; Hegedus et al., 2007) further show a linear correlation between F^{tet} and IR and between F^{tet} and CSA^{mean}. Consequently, F^{tet}, IR and CSA^{mean} are measurable, consistent, and linearly related measures of S_{mU} in animals, as summarized in Table 2.

Table 2. Measurable indices of MN and mU sizes in mammals. S_{MN} and S_{mU} are conceptual parameters which are adequately described by the measurable and linearly inter-related quantities reported in this table.

MN size ($\boldsymbol{S_{MN}}$)	mU size ($\boldsymbol{S_{mU}}$)
$\boldsymbol{S_{neuron}}$	F^{tet}
$\boldsymbol{D_{soma}}$	IR
	CSA^{mean}
	CSA^{tot}

Relationships between MN and mU properties

To assess whether the size-dependent relationships $A = k_c \cdot S_{MN}^c$ derived in this study were in accordance with Henneman's size principle of motor unit recruitment, we identified a set of experimental studies that concurrently measured a MN property B_{MN} (Table 1) and a muscle unit (mU) property A_{mU} for the same MU. The normalized global datasets obtained for the pairs $\{A_{mU}; B_{MN}\}$ were fitted with power trendlines, as previously described for MN properties, yielding $A_{mU} = k \cdot B_{MN}^b$ relationships. Using both the definition of S_{mU} (Table 2) and the $A = k_c \cdot S_{MN}^c$ relationships derived previously, the $A_{mU} = k \cdot B_{MN}^b$ relationships were then mathematically transformed into $S_{mU} = k \cdot S_{MN}^c$ relationships. If all c-values obtained from different $\{A_{mU}; B_{MN}\}$ pairs were of the same sign, it was concluded that mU and MN sizes were monotonically related. Considering the limited data available obtained from the literature, data obtained for MNs innervating different hindlimb muscles were merged. Also, cat, rat and mouse studies were processed independently but the resulting c-values were compared without regards to the related species.

Results

We respectively identified 18, 6 and 4 eligible studies on cats, rats and mice that reported processable experimental data for the morphometric and electrophysiological properties listed in Table 1. Additional eligible studies including some from the past 10 years were identified but could not be included in the meta-analysis as no processable data could be recovered. An additional 14 studies were found to perform concurrent MN and mU measurements on individual motor units.

From the cat eligible studies, the 17 pairs of MN properties and the 8 pairs of one MN and one mU property represented in the bubble diagram of Figure 2(A) were investigated.

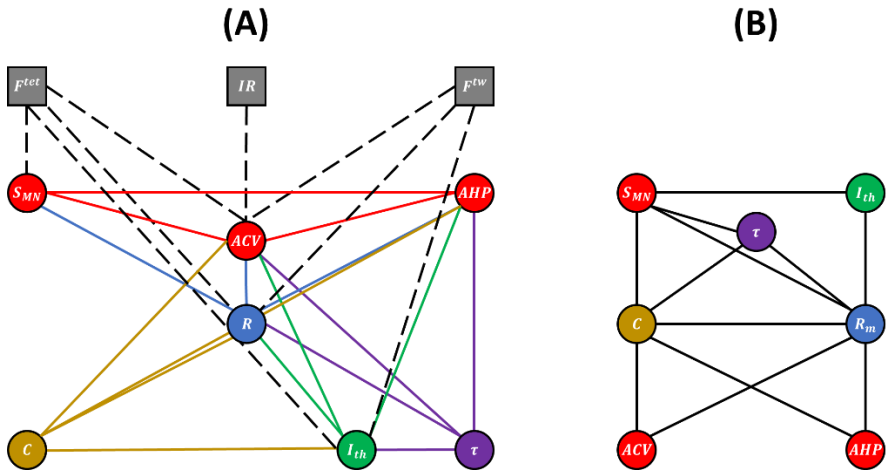

Figure 2. Experimental (A) and unknown (B) relations between MN and mU properties. (A) Bubble diagram representing the pairs of MN and/or mU properties that could be investigated in this study from the results provided by the 40 eligible studies. MN and mU properties are represented in circle and square bubbles, respectively. Relationships between MN properties are represented by coloured connecting lines; the colours red, blue, green, yellow, and purple are consistent with the order $ACV, AHP, R, I_{th}, C, \tau$ in which the pairs were investigated (see Table 3 for mathematical relationships). Relationships between one MN and one mU property are represented by black dashed lines. (B) Bubble diagram representing the mathematical relationships proposed in this study between pairs of MN properties for which no concurrent experimental data has been measured to date.

Relationships between MN properties

<u>Cat eligible studies</u>

All 18 eligible studies on cats included in this meta-analysis were published between 1966 and 2001. They applied similar experimental protocols. Briefly, animals were anesthetized, immobilized, and kept under artificial breathing. Hindlimb muscles of interest were dissected free and their nerves were mounted onto stimulating electrodes, while maintaining body temperature between 35°C and 38°C. After a laminectomy was performed over the lumbosacral region of the spinal cord, the MNs were

347 identified by antidromic invasion following electrical stimulation of the corresponding muscle nerves.
348 All studies reported the use of electrodes having stable resistances and being able to pass currents up
349 to 10 nA without evident polarization or rectification. Most studies performed intracellular recordings
350 using similar experimental approaches for the measurements of the electrophysiological parameters.
351 For instance, all studies measured the MN membrane input resistance using the spike height method
352 (Frank & Fuortes, 1956) by measuring the effects of steady currents, injected through the intracellular
353 microelectrode, on the amplitude of antidromic spikes. Some aspects of the experimental protocol
354 however diverged between studies, such as the age and the sex of the group of adult cats, the size
355 population of cats and recorded MNs, the muscles innervated by the recorded MNs, the means of
356 anaesthesia, the level of oxygen, and whether the spinal dorsal roots were severed (Kernell, 1966;
357 Burke, 1968; Barrett & Crill, 1974; Fleshman et al., 1981; Gustafsson & Pinter, 1984a; Gustafsson &
358 Pinter, 1984b; Zengel et al., 1985; Foehring et al., 1987), the complete surrounding hindlimbs were
359 denervated (Burke, 1968; Kernell & Zwaagstra, 1981) or the spinal cord was transected (Burke, 1968;
360 Krawitz et al., 2001). All the eligible studies performing morphometric measurements injected the
361 recorded MNs intracellularly with horseradish peroxidase (HRP) tracer by applying a continuous train
362 of anodal current pulses. The spinal cord was eventually sliced frozen or at room temperature with a
363 microtome or a vibratome and the MN morphometry was investigated. All morphometric
364 measurements were manually performed, and the MN compartments (soma, dendrites, axon)
365 approached by simple geometrical shapes, yielding the limitations previously listed.

366 Normalized relationships

367 The experimental data retrieved for the 17 pairs of MN properties drawn in Figure 2(A) were
368 successfully digitized and merged into 17 normalized global datasets as reproduced in Figure 3. For
369 information, power trendlines were fitted to these normalized datasets and reported in Table 3. All 17
370 trendlines were statistically significant, showing inter-study consistency in normalized measurements,
371 and adequately represented by a power model $A = k_a \cdot B^a$ (p-value$< 10^{-5}$ and $r^2 \in [0.34; 0.72]$ for
372 15 datasets; p-value $< 10^{-5}$ and $r^2 \in \{0.24; 0.17\}$ for the $\{C; AHP\}$ and $\{C; CV\}$ datasets
373 respectively).

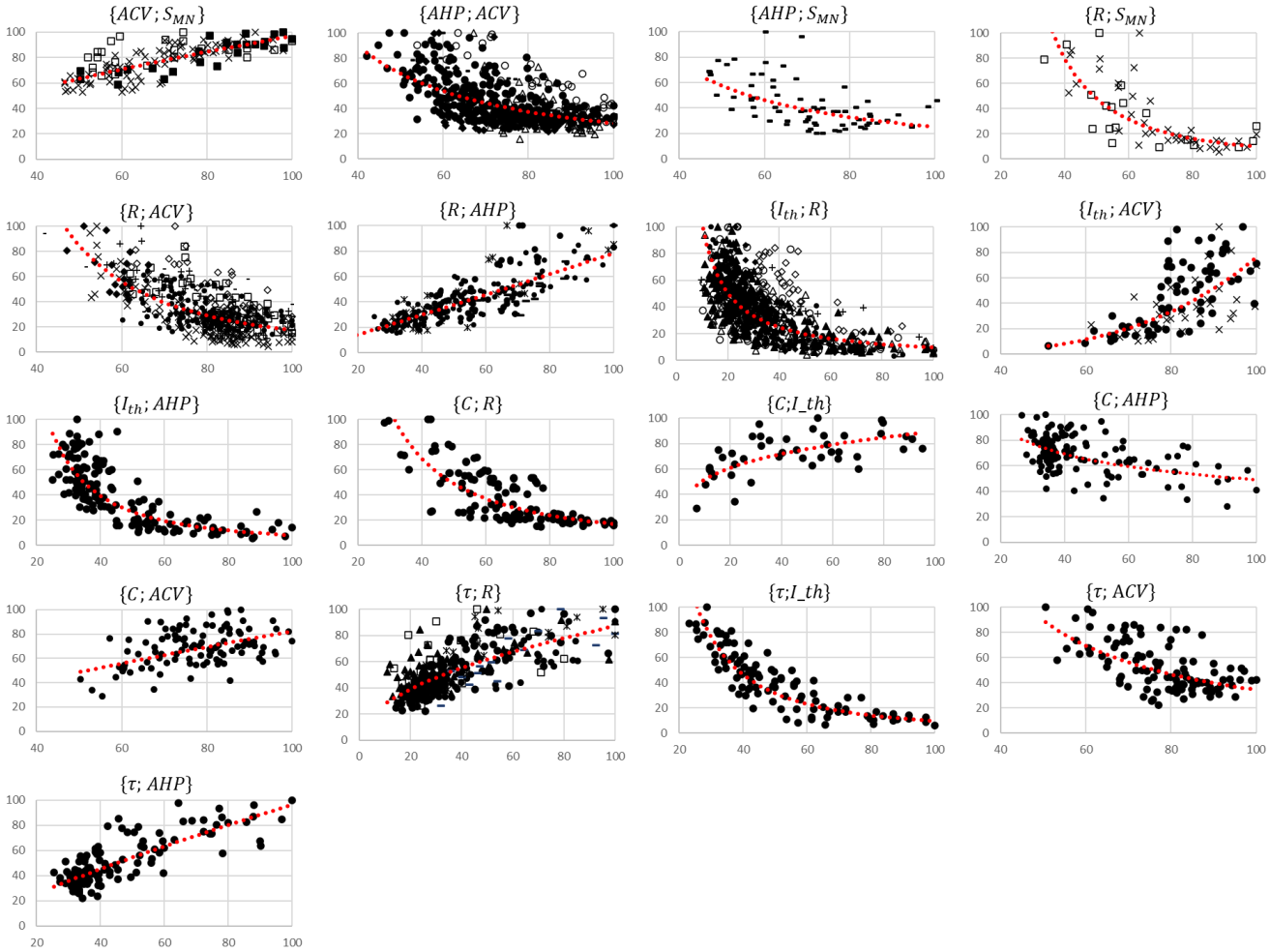

Figure 3. Normalized global datasets. These are obtained from the 18 eligible studies on cats that measured and investigated the 17 pairs of MN properties reported in Figure 2(A). For each $\{A; B\}$ pair, the property A is read on the y axis and B on the x axis. For information, power trendlines $A = k \cdot B^a$ (red dotted curves) are fitted to the data of each dataset and reported in Table 3. The studies are identified with the following symbols: • (Gustafsson, B., 1979; Gustafsson & Pinter, 1984a; Gustafsson & Pinter, 1984b), ○ (Munson et al., 1986), ▲ (Zengel et al., 1985), Δ (Foehring et al., 1987), ■ (Cullheim, 1978), □ (Burke, 1968; Burke & Ten Bruggencate, 1971; Burke et al., 1982), ◆ (Krawitz et al., 2001), ◇ (Fleshman et al., 1981), + (Kernell, 1966), X (Kernell & Zwaagstra, 1981; Kernell & Monster, 1981), - (Zwaagstra, B. & Kernell, 1980), — (Sasaki, 1991), ✶ (Pinter & Vanden Noven, 1989). The axes are given in % of the maximum retrieved values in the studies consistently with the Methods section.

The 17 normalized global datasets were processed according to the Methods to derive normalized mathematical relationships between the electrophysiological properties listed in Table 1 and MN size S_{MN}. First, the normalized size-dependent relationship $ACV = 4.0 \cdot S_{MN}^{0.7}$, reported in Table 3, was derived from the trendline fitting of the normalized $\{ACV; S_{MN}\}$ dataset, which was obtained from 3 studies (Cullheim, 1978; Kernell & Zwaagstra, 1981; Burke et al., 1982) and is represented in the upper-left panel in Figure 3. This resulted in a statistically significant relationship ($r^2 = 0.58$, p-value$< 10^{-5}$). A statistically significant ($r^2 = 0.59$, p-value$< 10^{-5}$) inverse relationship $S_{MN} = k_d \cdot ACV^d$ was also fitted to this dataset. Then, the $\{AHP; ACV\}$ dataset, represented in the second panel upper row in Figure 3 and obtained from 3 studies (Zwaagstra, B. & Kernell, 1980; Gustafsson & Pinter, 1984a; Foehring et al., 1987) was transformed into a new $\{AHP; S_{MN}\}_1$ dataset by applying the priory derived $S_{MN} = k_d \cdot ACV^d$ relationship to the list of ACV-values. This transformed $\{AHP; S_{MN}\}_1$ dataset was then merged with the $\{AHP; S_{MN}\}_2$ dataset (third panel upper row in Figure 2) obtained from (Zwaagstra, B. & Kernell, 1980), yielding the final $\{AHP; S_{MN}\}_f$ dataset of $N = 492$ data points shown in Figure 4, second panel. A statistically significant ($r^2 = 0.58$, p-value$< 10^{-5}$) power trendline $AHP = 2.5 \cdot 10^4 \cdot S_{MN}^{-1.5}$ was fitted to the $\{AHP; S_{MN}\}_f$ dataset and is reported in Table 3. As before, a statistically significant ($r^2 = 0.38$, p-value$< 10^{-5}$) inverse relationship $S_{MN} = k_d \cdot AHP^d$ was also fitted to this dataset for future use. A similar procedure was applied to derive the normalized final relationships between $\{R, I_{th}, C, \tau\}$ and S_{MN} reported in the last column of Table 3. A statistically significant (p-value$< 10^{-5}$) correlation was obtained between each electrophysiological property $\{ACV, AHP, R, I_{th}, C, \tau\}$ and S_{MN} as reported in Table 3. With $r^2 \in [0.28; 0.58]$, it was obtained that $\{I_{th}, C, CV\}$ and $\{R, AHP, \tau\}$ respectively increased and decreased with increasing MN sizes S_{MN}, with slopes reported in Table 3 and visually displayed in Figure 5.

Table 3. Fitted experimental data of pairs of MN properties and subsequent normalized final size-related relationships. For information, the r^2, p-value and the equation $A = k_a \cdot B^a$ are reported for each fitted global dataset. The normalized MN-size dependent relationships $A = k_c \cdot S_{MN}^c$ are mathematically derived from the transformation of the global datasets and from the power trendline fitting of the final datasets (N data points) as described in the Methods.

MN property	$\boldsymbol{A = k_a \cdot B^a}$ (normalized global datasets)						$\boldsymbol{A = k_c \cdot S_{MN}^c}$ (final MN-size dependent datasets)				
$\boldsymbol{A}$	Relationship	k_a	a	r^2	p-value	Reference studies	k_c	c	r^2	p-value	N points
$\boldsymbol{ACV}$	$ACV = k_a \cdot S_{MN}^a$	4.0	0.7	0.58	$p < 10^{-5}$	(Cullheim, 1978; Kernell & Zwaagstra, 1981; Burke et al., 1982)	4.0	0.7	0.58	$p < 10^{-5}$	109
$\boldsymbol{AHP}$	$AHP = k_a \cdot S_{MN}^a$	$6.1 \cdot 10^3$	-1.2	0.34	$p < 10^{-5}$	(Zwaagstra, B. & Kernell, 1980)	$2.5 \cdot 10^4$	-1.5	0.41	$p < 10^{-5}$	492
	$AHP = k_a \cdot ACV^a$	$1.5 \cdot 10^4$	-1.4	0.43	$p < 10^{-5}$	(Zwaagstra, B. & Kernell, 1980; Gustafsson & Pinter, 1984a; Foehring et al., 1987)					
$\boldsymbol{R}$	$R = k_a \cdot S_{MN}^a$	$1.5 \cdot 10^5$	-2.1	0.61	$p < 10^{-5}$	(Kernell & Zwaagstra, 1981; Burke et al., 1982)	$9.6 \cdot 10^5$	-2.4	0.37	$p < 10^{-5}$	745
	$R = k_a \cdot ACV^a$	$6.3 \cdot 10^4$	-2.3	0.40	$p < 10^{-5}$	(Kernell, 1966; Burke, 1968; Barrett & Crill, 1974; Kernell & Zwaagstra, 1981; Fleshman et al., 1981; Gustafsson & Pinter, 1984a; Sasaki, 1991)					
	$R = k_a \cdot AHP^a$	$6.2 \cdot 10^{-1}$	1.1	0.65	$p < 10^{-5}$	(Gustafsson, B., 1979; Gustafsson & Pinter, 1984a; Foehring et al., 1987; Pinter & Vanden Noven, 1989; Sasaki, 1991)					
$\boldsymbol{I_{th}}$	$I_{th} = k_a \cdot R^a$	$1.1 \cdot 10^3$	-1.0	0.37	$p < 10^{-5}$	(Kernell, 1966; Fleshman et al., 1981; Gustafsson & Pinter, 1984b; Zengel et al., 1985; Munson et al., 1986; Foehring et al., 1987; Krawitz et al., 2001)	$9.0 \cdot 10^{-4}$	2.5	0.37	$p < 10^{-5}$	722
	$I_{th} = k_a \cdot ACV^a$	$3.2 \cdot 10^{-6}$	3.7	0.37	$p < 10^{-5}$	(Kernell & Monster, 1981; Gustafsson & Pinter, 1984b)					
	$I_{th} = k_a \cdot AHP^a$	$2.5 \cdot 10^4$	-1.7	0.60	$p < 10^{-5}$	(Gustafsson & Pinter, 1984b)					
$\boldsymbol{C}$	$C = k_a \cdot R^a$	$2.4 \cdot 10^2$	-0.4	0.57	$p < 10^{-5}$	(Gustafsson & Pinter, 1984a)	1.2	1.0	0.28	$p < 10^{-5}$	444
	$C = k_a \cdot I_{th}^a$	$2.9 \cdot 10^1$	0.26	0.51	$p < 10^{-5}$	(Gustafsson & Pinter, 1984b)					
	$C = k_a \cdot AHP^a$	$2.8 \cdot 10^2$	-0.4	0.24	$p < 10^{-5}$	(Gustafsson & Pinter, 1984a)					
	$C = k_a \cdot ACV^a$	2.5	0.8	0.17	$p < 10^{-5}$	(Gustafsson & Pinter, 1984a)					
$\boldsymbol{\tau}$	$\tau = k_a \cdot R^a$	8.7	0.5	0.52	$p < 10^{-5}$	(Burke & Ten Bruggencate, 1971; Barrett & Crill, 1974; Gustafsson, B., 1979; Gustafsson & Pinter, 1984a; Zengel et al., 1985; Pinter & Vanden Noven, 1989; Sasaki, 1991)	$2.6 \cdot 10^4$	-1.5	0.46	$p < 10^{-5}$	649
	$\tau = k_a \cdot AHP^a$	2.2	0.8	0.63	$p < 10^{-5}$	(Gustafsson & Pinter, 1984a)					
	$\tau = k_a \cdot I_{th}^a$	$2.3 \cdot 10^2$	-0.45	0.72	$p < 10^{-5}$	(Gustafsson & Pinter, 1984b)					
	$\tau = k_a \cdot ACV^a$	$1.2 \cdot 10^4$	-1.3	0.30	$p < 10^{-5}$	(Gustafsson & Pinter, 1984a)					

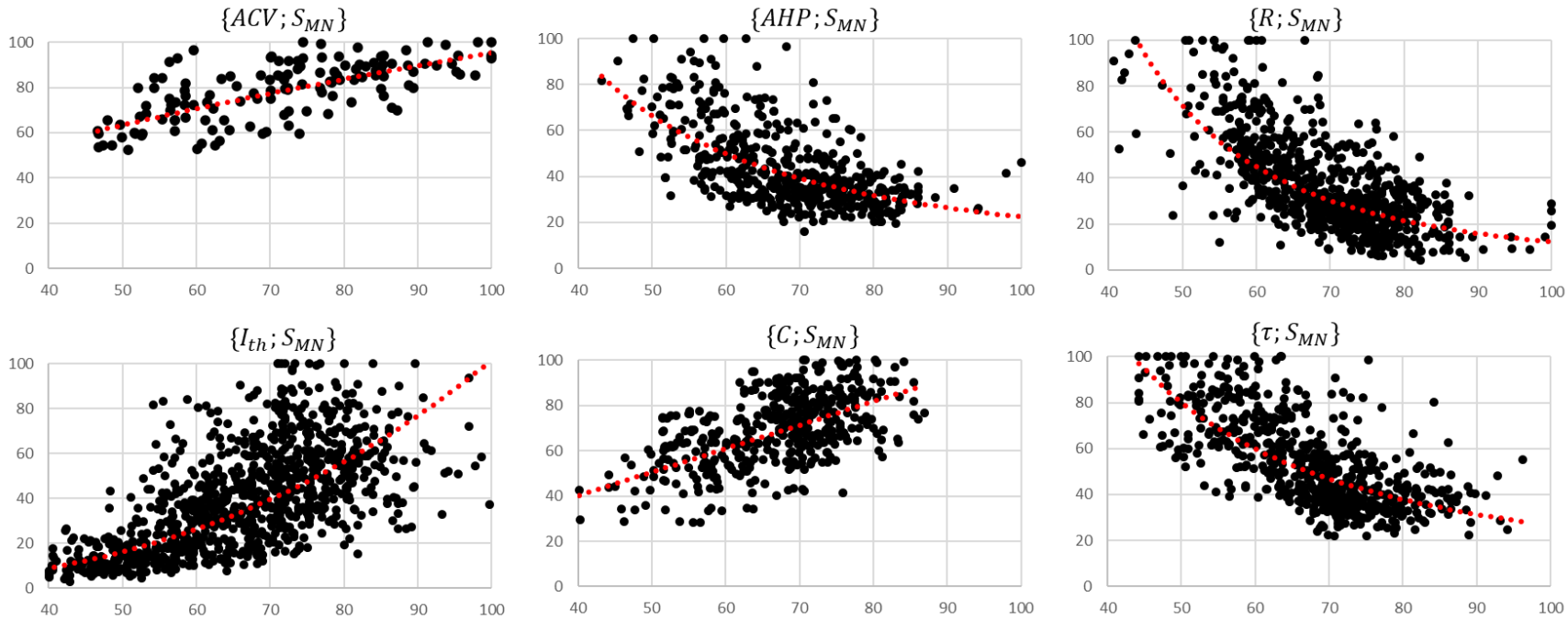

Figure 4. Normalized MN size-related final datasets. These are obtained from the 18 eligible studies on cats that concurrently measured at least two of the morphometric and electrophysiological properties listed in Table 1. For each $\{A; S_{MN}\}$ pair, the property A is read on the y axis and S_{MN} on the x axis. The power trendlines $A = k_c \cdot S_{MN}^c$ (red dotted curves) are fitted to each dataset and are reported in Table 3.

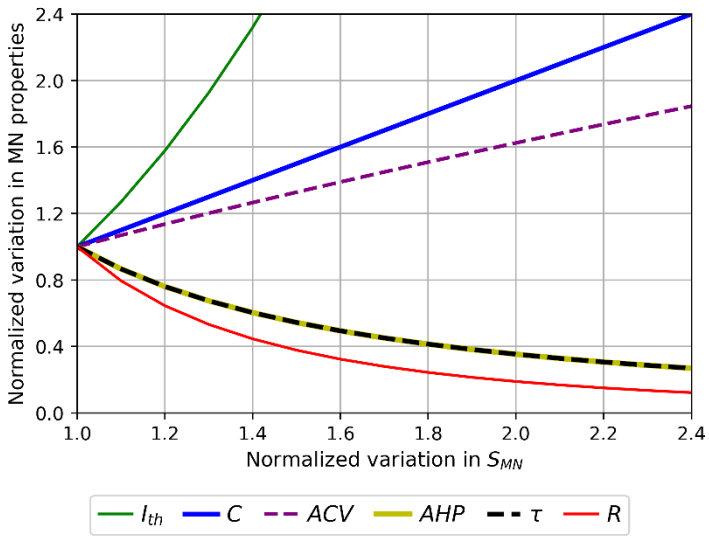

Figure 5. Normalized size-dependent behaviour of the MN properties ACV, AHP, R, I_{th}, C and τ. For displaying purposes, the MN properties are plotted in arbitrary units as power functions (intercept $k = 1$) of S_{MN}: $A = S_{MN}^{c}$ according to Table 3. The larger the MN size, the larger ACV, C and I_{th} in the order of increasing slopes, and the lower AHP, τ and R in the order of increasing slopes.

Normalized mathematical relationships between electrophysiological properties

The final size-dependent relationships reported in Table 3 were mathematically combined to yield normalized relationships between all electrophysiological properties listed in Table 1. As an example, $I_{th} = 9.4 \cdot 10^{-4} \cdot S_{MN}^{2.5}$ and $R = 9.6 \cdot 10^{5} \cdot S_{MN}^{-2.4}$ were obtained in Table 3. When mathematically combined (with the latter mathematically inverted as $S_{MN} = 2.9 \cdot 10^{2} \cdot R^{-0.4}$), these relationships yielded the normalized relationship between rheobase and input resistance $I_{th} = 1.5 \cdot 10^{3} \cdot R^{-1}$. All normalized relationships between MN electrophysiological properties hence obtained are provided in Supplementary Material.

Validation of the normalized relationships

The procedure and normalized relationships reported in Table 3 were obtained from the complete global datasets represented in Figure 3. To provide a validation of this approach and of the normalized relationships, the global datasets were split into two random partitions respectively containing 70% and 30% of the data, after the data points order was randomized within each dataset. Normalized relationships between $\{CV, AHP, R, I_{th}, C, \tau\}$ and S_{MN}, and then between all electrophysiological properties were derived from the 70%-datasets following the same procedure as previously described, and their predictions compared to the ground truth 30%-datasets with calculations of the $nME, nRMSE$ and r_{pred}^{2} validation metrics. This validation was performed for five random 70%-30% partitions of the global datasets. Figure 6 reports the average $nME, nRMSE$ and r_{pred}^{2} values across the five trials. The coefficient of determination between experimental and predicted quantities was

besides compared to the r^2_{exp}-value of the power trendline best fitted to the experimental data directly, which provides the highest r^2 value possibly reachable by our model. As displayed in Figure 6, the normalized relationships obtained from the 17 70%-datasets predicted the experimental data from the 30%-datasets with average nME between 48% and 412%, 12% to 26% $nRMSE$ and coefficients of determination r^2_{pred} that diverged from the higher limit r^2_{exp} by a maximum of 7% (for the $\{R; ACV\}$ pair in Figure 6). These results confirm the validity of the obtained relationships.

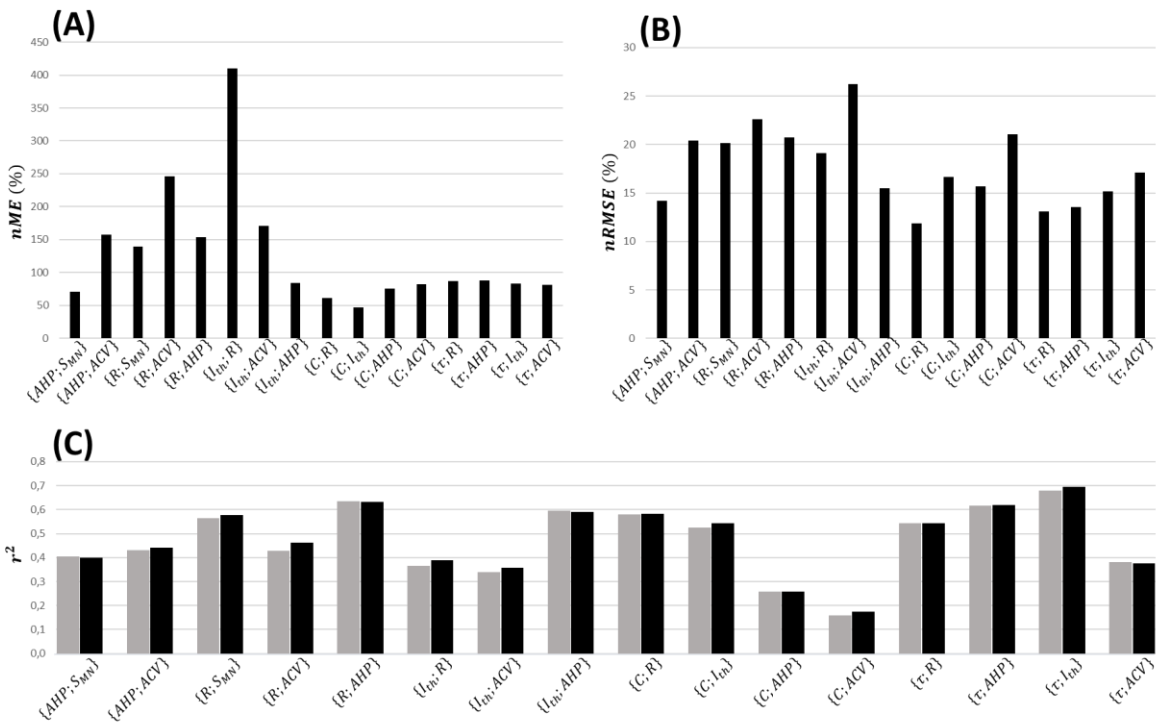

Figure 6. Validation of the normalized mathematical relationships obtained from the 70%-datasets against the corresponding 30%-datasets. For each 30%-dataset are reported the average values across the five trials of (A) the normalized maximum error (nME), (B) the normalized root-mean-square error ($nRMSE$), and (C) coefficient of determination (r^2_{pred}, grey bars) which is compared with the coefficient of determination (r^2_{exp}, black bars) of the power trendline fitted to the experimental data directly.

The normalized relationships reported in Supplementary material (and in Table 6 after scaling) were also strongly consistent with other experimental data in cats that were not included in the global datasets displayed in Figure 3 and used for deriving the normalized relationships. The normalized relationships $I^{th} = k \cdot \tau^{-1.7}$, $\frac{1}{C} = k \cdot \tau^{0.6}$, $\frac{1}{S_{MN}} = k \cdot CV^{-1.4}$ and $\frac{1}{R} = k \cdot CV^{3.5}$ yielded, when combined, $\frac{I^{th}}{C} = k \cdot \tau^{-1.1}$ and $\frac{1}{R \cdot S_{MN}} = k \cdot CV^{2.1}$, which are consistent with the relationship $\frac{I^{th}}{C} = k \cdot \tau^{-1}$ experimentally observed by Gustafsson & Pinter (1985) and $\frac{1}{R \cdot S_{MN}} = k \cdot CV^{1.9}$ measured by Kernell & Zwaagstra (1981). The stronger-than-linear inverse relationship $R = k \cdot S_{MN}^{-2.4}$ is also consistent with the phenomenological conclusions by Kernell & Zwaagstra (1981).

456 Scaling of the normalized relationships

457 The normalized relationships provided in Supplementary Material were finally scaled to typical cat data
458 obtained from the literature following the procedure described in the Methods section. D_{soma} and
459 S_{neuron} were found to vary in cats over an average $q_S^E = 2.4$-fold range according to a review of the
460 morphometric studies reported in the two first lines of Table 4. The similar ranges obtained for these
461 two morphometric quantities support the findings of the linear inter-relationship existing between
462 them and justified in the Methods.

463 It must however be noted that the minimum and maximum values of S_{neuron} and D_{soma} reported in
464 Table 4 may underestimate the true distribution of MN sizes in a MN pool for several reasons. First,
465 the studies reported in Table 4 investigated MN populations of small size, so that the largest and
466 smallest MNs of the investigated MN pools may not have been systematically identified and measured.
467 Also, dendritic labelling by staining may only identify dendrites up to the 3rd dendritic branch (Issa et
468 al., 2010; Fogarty et al., 2018) and full dendritic trees may not be identified, thus underestimating
469 S_{neuron} for the largest MNs that exhibit the highest dendritic tree complexity (Fogarty et al., 2020).
470 Finally, the distribution of gamma- and alpha-MN sizes is typically bimodal and the size distributions
471 of the two populations are reported to overlap (Moschovakis et al., 1991; von Steyern et al., 1999;
472 Friese et al., 2009; Deardorff et al., 2013). However, most studies reported in Table 4 identify the alpha
473 MNs from the gamma MNs by visually splitting the bimodal distributions of MN sizes in two
474 independent domains (Donselaar et al., 1986; Ishihara et al., 2001), thus neglecting the overlap.
475 Similarly, some studies identify as gamma MNs any MN showing an axonal conduction velocity typically
476 less than $\sim 60 m \cdot s^{-1}$ (Zwaagstra, B. & Kernell, 1980; Ulfhake, B. & Kellerth, 1984). These approaches
477 lead to overestimating the lower limit for the reported D_{soma} and S_{neuron} values. Consequently, true
478 ranges in MN sizes may be larger than the theoretical ones reported in Table 4. A similar comment can
479 be made for the electrophysiological properties reported in Table 5.

480 However, the $q_S^E = 2.4$-fold range obtained for cats is consistent with the fold-ranges obtained from
481 rat and mouse data for D_{soma} as reported in Table 4, while it underestimates the 4.4-fold range in
482 S_{neuron} values observed in mice. Table 4 finally shows that typical cat MN sizes are larger than in rats
483 and mice respectively, as reviewed by Manuel et al. (2019).

484

Table 4. Typical ranges of physiological values for $\boldsymbol{D_{soma}}$ and $\boldsymbol{S_{neuron}}$ in cat rat and mouse species. S_{MN} is found to vary over an average $q_S^E = 2.4$-fold range, which sets the amplitude of the theoretical ranges. Absolute {min; max} reports the minimum and maximum values retrieved in the reference studies for D_{soma} and S_{neuron}, while average {min; max} is obtained as the average across reference studies of minimum and maximum values retrieved per study.

	Property	Unit	Absolute {min;max}	Average {min; max}	q_S^E	Reference studies	Theoretical range
Cat	$\boldsymbol{D_{soma}}$	$[\mu m]$	$\{25.0; 90.0\}$	$\{36.7; 75.5\}$	2.2	(Kernell, 1966; Cullheim, 1978; Zwaagstra, B. & Kernell, 1980; Kernell & Zwaagstra, 1981; Ulfhake & Kellerth, 1981; Zwaagstra & Kernell, 1981; Burke et al., 1982; Donselaar et al., 1986; Destombes et al., 1992)	$[33; 79]$
	$\boldsymbol{S_{neuron}}$	$[mm^2]$	$\{0.08; 0.64\}$	$\{0.17; 0.45\}$	2.7	(Barrett & Crill, 1974; Ulfhake & Kellerth, 1981; Burke et al., 1982; Ulfhake, B. & Kellerth, 1984; Ulfhake, Brun & Cullheim, 1988; Moschovakis et al., 1991)	$[0.18; 0.44]$
Rat	$\boldsymbol{D_{soma}}$	$[\mu m]$	$\{17.5; 66.0\}$	$\{23.9; 55.7\}$	2.4	(Swett et al., 1986; von Steyern et al., 1999; Copray & Kernell, 2000; Ishihara et al., 2001; Deardorff et al., 2013; Mierzejewska-Krzyżowska et al., 2014)	
Mouse	$\boldsymbol{D_{soma}}$	$[\mu m]$	$\{14.0; 35.0\}$	$\{14.0; 35.0\}$	2.5	(von Steyern et al., 1999)	
	$\boldsymbol{S_{neuron}}$	$[mm^2]$	$\{0.01; 0.08\}$	$\{0.01; 0.06\}$	4.4	(Amendola & Durand, 2008; Brandenburg et al., 2020)	

Then, the empirical q_A^E and theoretical q_A^T ratios, defined in the Methods, were calculated for each MN electrophysiological property A and are reported in Table 5. For example, MN resistance R was found to vary over an average $q_R^E = 10.9$-fold range in a MN pool according to the literature, while the theoretical fold range $q_R^T = (q_S^E)^{|c_R|} = 2.4^{2.4} = 8.4$ was obtained from the $R = 9.6 \cdot 10^5 \cdot S_{MN}^{-2.4}$ normalized relationship previously derived when a 2.4-fold range is set for S_{MN}. As shown in Table 5, $\frac{q_A^E}{q_A^T} \in [0.8; 1.3]$ for the MN properties $C, \tau,\ AHP$ and ACV, while the theoretical ranges for R and I_{th} span over a narrower domain than expected from experimental results. The latter either suggests an underestimation of the MN q_S^E-fold range as discussed previously or of the power c in the relationships $I_{th}, R = k_c \cdot S_{MN}^c$.

Table 5: Typical ranges of physiological values for the MN properties $\boldsymbol{R}, \boldsymbol{R_m}, \boldsymbol{C}, \boldsymbol{\tau}, \boldsymbol{I_{th}}, \boldsymbol{AHP}$ and $\boldsymbol{ACV}$. As described in the Methods section, q_A^E is the average among reference studies of the ratios of minimum and maximum values; the properties experimentally vary over a q_A^E-fold range. This ratio compares with the theoretical ratio $q_A^T = (q_S^E)^{|c|}$ (with c taken from Table 3), which sets the amplitude of the theoretical ranges. Absolute and average {min; max} are obtained as described in Table 4.

MN property	Unit	Absolute exp {min;max}	Average exp {min; max}	$\boldsymbol{q_A^E}$	Reference studies	$\boldsymbol{q_A^T}$	$\boldsymbol{\frac{q_A^E}{q_A^T}}$	Theoretical range
$\boldsymbol{R}$	$M\Omega$	$\{0.2; 8.1\}$	$\{0.4; 4.0\}$	10.9	(Kernell, 1966; Burke, 1968; Burke & Ten Bruggencate, 1971; Barrett & Crill, 1974; Gustafsson, B., 1979; Kernell & Zwaagstra, 1981; Fleshman et al., 1981; Burke et al., 1982; Ulfhake, B. & Kellerth, 1984; Gustafsson & Pinter, 1984a; Zengel et al., 1985; Foehring et al., 1986; Munson et al., 1986; Foehring et al., 1987; Sasaki, 1991; Krawitz et al., 2001)	8.4	1.3	$[0.5; 4.0]$
$\boldsymbol{C}$	nF	$\{2.2; 8.5\}$	$\{2.2; 8.5\}$	3.9	(Gustafsson & Pinter, 1984a; Gustafsson & Pinter, 1985)	2.3	1.6	$[3.2; 7.5]$
$\boldsymbol{\tau}$	ms	$\{2.0; 14.2\}$	$\{2.9; 10.2\}$	3.5	(Burke & Ten Bruggencate, 1971; Barrett & Crill, 1974; Gustafsson, B., 1979; Ulfhake, B. & Kellerth, 1984; Gustafsson & Pinter, 1984a; Gustafsson & Pinter, 1985; Sasaki, 1991)	3.7	0.9	$[2.8; 10.3]$
$\boldsymbol{I_{th}}$	nA	$\{1.7; 52.7\}$	$\{2.3; 36.6\}$	16.3	(Fleshman et al., 1981; Kernell & Monster, 1981; Ulfhake, B. & Kellerth, 1984; Gustafsson & Pinter, 1984b; Zengel et al., 1985; Foehring et al., 1986; Munson et al., 1986; Foehring et al., 1987; Krawitz et al., 2001)	9.1	1.8	$[3.9; 35.0]$
$\boldsymbol{AHP}$	ms	$\{10.6; 266.6\}$	$\{44.2; 158.7\}$	4.1	(Eccles et al., 1957; Gustafsson, B., 1979; Dum & Kennedy, 1980; Zwaagstra, B. & Kernell, 1980; Ulfhake, B. & Kellerth, 1984; Gustafsson & Pinter, 1984a; Zengel et al., 1985; Foehring et al., 1987; Sasaki, 1991)	3.8	1.1	$[42.6; 160.2]$
$\boldsymbol{ACV}$	$m \cdot s^{-1}$	$\{51.1; 127.2\}$	$\{65.3; 114.8\}$	1.8	(Eccles et al., 1957; McPhedran et al., 1965; Kernell, 1966; Appelberg & Emonet-Dénand, 1967; Burke, 1968; Barrett & Crill, 1974; Proske & Waite, 1974; Bagust, 1974; Stephens & Stuart, 1975; Cullheim, 1978; Dum & Kennedy, 1980; Zwaagstra, B. & Kernell, 1980; Kernell & Zwaagstra, 1981; Fleshman et al., 1981; Glenn & Dement, 1981; Burke et al., 1982; Gustafsson & Pinter, 1984a; Zengel et al., 1985; Foehring et al., 1986; Foehring et al., 1987)	2.3	0.8	$[63.5; 116.6]$

The normalized relationships were finally scaled using the theoretical ranges reported in the last column of Table 5. Taking the $\{I_{th}; R\}$ pair as example, as $I_{th} = 1.4 \cdot 10^3 \cdot R^{-1}$ (normalized relationship derived previously and provided in Supplementary Material), $R \in [0.5; 4.0] \cdot 10^6 \Omega$ and

$I_{th} \in [3.9; 35.0] \cdot 10^{-9} A$ (Table 5), it was directly obtained from the Methods that $I_{th} = \frac{2.7 \cdot 10^{-2}}{R} = \frac{\Delta V^{th}}{I^{th}}$ in SI base units. A similar approach yielded the mathematical relationships reported in Table 6 between all MN electrophysiological and morphometric properties $ACV, AHP, R, I_{th}, C, \tau$ and S_{MN}. All constants and relationships are given in SI base units. The specific capacitance C_m and the membrane voltage threshold ΔV_{th} were found to be constant among MNs, a property discussed in the Discussion section.

<u>Specific resistance R_m</u>

A specific membrane input resistance is generally defined in the literature (Barrett & Crill, 1974; Burke et al., 1982; Kernell, 2006) as the surface input resistance $R = \frac{R_m}{S_{neuron}}$. According to the relationships in Table 6, we obtain $R = \frac{R_m}{S_{neuron}} = \frac{1.7 \cdot 10^{-10}}{S_{neuron}^{2.4}}$, which yields $R_m = \frac{1.7 \cdot 10^{-10}}{S_{neuron}^{1.4}}$. This finding is consistent with the conclusions from Barrett & Crill (1974), who reported a weak but significant linear relationship between R_m and $1/S_{MN}$. Also, $R_m = \frac{1.7 \cdot 10^{-10}}{S_{MN}^{1.4}}$ yields $R_m = 4.1 \cdot AHP^{0.9}$ from the relationships in Table 6, which is consistent with the indirect conclusion of a positive correlation between R_m and AHP in Gustafsson & Pinter (1984b). Finally, considering that $q_S^E = 2.4$ and $S_{neuron} \in [0.18; 0.44]\ mm^2$ (Table 4), $R_m = \frac{1.7 \cdot 10^{-10}}{S_{MN}^{1.4}}$ yields that R_m varies over the q_A^E =3.5-fold theoretical range $[0.21; 0.73]\ \Omega \cdot m^2$. This is both consistent with the $q_A^E = 3.2$-fold range and the $\left[A_{min}^E;\ A_{max}^E\right] = [0.16; 0.62]\ \Omega \cdot m^2$ mean range previously speculated in the literature (Albuquerque & Thesleff, 1968; Barrett & Crill, 1974; Burke et al., 1982; Gustafsson & Pinter, 1984a; Kernell & Zwaagstra, 1989). The MN property R_m was therefore added to Table 6.

Table 6. Mathematical empirical cat relationships between the MN properties $S_{neuron}, D_{soma}, R, R_m, C, \tau, I^{th}$, AHP and ACV. Each column provides the relationships between one and the nine other MN properties. If one property is known, the complete MN profile can be reconstructed by using the pertinent line in this table. All constants and properties are provided in SI base units (meters, seconds, ohms, farads and ampers). These relationships were obtained for alpha-MNs innervating the hindlimbs of adult cats in vivo.

	$S_{neuron}[m^2]$	$D_{soma}[m]$	$R[\Omega]$	$R_m[\Omega \cdot m^2]$	$C[F]$	$\tau[s]$	$I_{th}[A]$	$AHP[s]$	$ACV[m \cdot s^{-1}]$
$S_{neuron}[m^2]$		$D_{soma} = 1.8 \cdot 10^2 \cdot S_{neuron}$	$R = \frac{1.7 \cdot 10^{-10}}{S_{neuron}^{2.4}}$	$R_m = \frac{1.7 \cdot 10^{-10}}{S_{neuron}^{1.4}}$	$C = 1.0 \cdot 10^{-2} \cdot S_{neuron}$	$\tau = \frac{1.0 \cdot 10^{-12}}{S_{neuron}^{1.5}}$	$I_{th} = 3.8 \cdot 10^8 \cdot S_{neuron}^{2.5}$	$AHP = \frac{1.0 \cdot 10^{-11}}{S_{neuron}^{1.5}}$	$ACV = 3.0 \cdot 10^6 \cdot S_{neuron}^{0.7}$
$D_{soma}[m]$	$S_{neuron} = 5.5 \cdot 10^{-3} \cdot D_{soma}$		$R = \frac{5.1 \cdot 10^{-5}}{D_{soma}^{2.4}}$	$R_m = \frac{2.8 \cdot 10^{-7}}{D_{soma}^{1.4}}$	$C = 6.7 \cdot 10^{-5} \cdot D_{soma}$	$\tau = \frac{2.3 \cdot 10^{-9}}{D_{soma}^{1.5}}$	$I_{th} = 7.8 \cdot 10^2 \cdot D_{soma}^{2.5}$	$AHP = \frac{2.7 \cdot 10^{-8}}{D_{soma}^{1.5}}$	$ACV = 8.1 \cdot 10^4 \cdot D_{soma}^{0.7}$
$R[\Omega]$	$S_{neuron} = \frac{9.5 \cdot 10^{-5}}{R^{0.4}}$	$D_{soma} = \frac{1.7 \cdot 10^{-2}}{R^{0.4}}$		$R_m = 9.5 \cdot 10^{-5} \cdot R^{0.6}$	$C = \frac{1.3 \cdot 10^{-6}}{R^{0.4}}$	$\tau = 9.6 \cdot 10^{-7} \cdot R^{0.6}$	$I_{th} = \frac{2.7 \cdot 10^{-2}}{R}$	$AHP = 1.3 \cdot 10^{-5} \cdot R^{0.6}$	$ACV = \frac{4.9 \cdot 10^3}{R^{0.3}}$
$R_m[\Omega \cdot m^2]$	$S_{neuron} = \frac{1.5 \cdot 10^{-7}}{R_m^{0.7}}$	$D_{soma} = \frac{2.6 \cdot 10^{-5}}{R_m^{0.7}}$	$R = 6.8 \cdot 10^6 \cdot R_m^{1.7}$		$C = \frac{2.6 \cdot 10^{-9}}{R_m^{0.7}}$	$\tau = 1.4 \cdot 10^{-2} \cdot R_m$	$I_{th} = \frac{2.2 \cdot 10^{-9}}{R_m^{1.8}}$	$AHP = 2.2 \cdot 10^{-1} \cdot R_m^{1.1}$	$ACV = \frac{5.4 \cdot 10^1}{R_m^{0.5}}$
$C[F]$	$S_{neuron} = 1.2 \cdot 10^2 \cdot C$	$D_{soma} = 2.1 \cdot 10^4 \cdot C$	$R = \frac{1.5 \cdot 10^{-15}}{C^{2.5}}$	$R_m = \frac{1.8 \cdot 10^{-13}}{C^{1.5}}$		$\tau = \frac{8.6 \cdot 10^{-16}}{C^{1.5}}$	$I_{th} = 6.5 \cdot 10^{13} \cdot C^{2.6}$	$AHP = \frac{7.7 \cdot 10^{-15}}{C^{1.6}}$	$ACV = 8.2 \cdot 10^7 \cdot C^{0.7}$
$\tau[s]$	$S_{neuron} = \frac{8.4 \cdot 10^{-9}}{\tau^{0.7}}$	$D_{soma} = \frac{1.5 \cdot 10^{-6}}{\tau^{0.7}}$	$R = 7.1 \cdot 10^9 \cdot \tau^{1.6}$	$R_m = 6.0 \cdot 10^1 \cdot \tau$	$C = \frac{1.6 \cdot 10^{-10}}{\tau^{0.6}}$		$I_{th} = \frac{1.6 \cdot 10^{-12}}{\tau^{1.7}}$	$AHP = 1.7 \cdot 10^1 \cdot \tau$	$ACV = \frac{7.5}{\tau^{0.5}}$
$I_{th}[A]$	$S_{neuron} = 4.0 \cdot 10^{-4} \cdot I_{th}^{0.4}$	$D_{soma} = 7.1 \cdot 10^{-2} \cdot I_{th}^{0.4}$	$R = \frac{3.1 \cdot 10^{-2}}{I_{th}}$	$R_m = \frac{1.2 \cdot 10^{-5}}{I_{th}^{0.6}}$	$C = 5.3 \cdot 10^{-6} \cdot I_{th}^{0.4}$	$\tau = \frac{1.2 \cdot 10^{-7}}{I_{th}^{0.6}}$		$AHP = \frac{1.5 \cdot 10^{-6}}{I_{th}^{0.6}}$	$ACV = 1.3 \cdot 10^4 \cdot I_{th}^{0.3}$
$AHP[s]$	$S_{neuron} = \frac{5.5 \cdot 10^{-8}}{AHP^{0.7}}$	$D_{soma} = \frac{9.8 \cdot 10^{-6}}{AHP^{0.7}}$	$R = 7.5 \cdot 10^7 \cdot AHP^{1.6}$	$R_m = 4.1 \cdot AHP^{0.9}$	$C = \frac{1.0 * 10^{-9}}{AHP^{0.6}}$	$\tau = 6.2 \cdot 10^{-2} \cdot AHP$	$I_{th} = \frac{1.8 * 10^{-10}}{AHP^{1.7}}$		$ACV = \frac{2.7 \cdot 10^1}{AHP^{0.5}}$
$ACV[m \cdot s^{-1}]$	$S_{neuron} = 4.6 \cdot 10^{-10} \cdot ACV^{1.4}$	$D_{soma} = 8.3 \cdot 10^{-8} \cdot ACV^{1.4}$	$R = \frac{8.3 \cdot 10^{12}}{ACV^{3.5}}$	$R_m = \frac{3.8 \cdot 10^3}{ACV^{2.1}}$	$C = 1.0 \cdot 10^{-11} \cdot ACV^{1.4}$	$\tau = \frac{7.4 \cdot 10^1}{ACV^{2.1}}$	$I_{th} = 1.1 \cdot 10^{-15} \cdot ACV^{3.6}$	$AHP = \frac{1.4 \cdot 10^3}{ACV^{2.2}}$	

Predicting correlations between MN properties

This study also predicts the correlations between MN properties that were either never reported in past review studies, such as the positive $S_{MN} - \tau$ relationship, or never concurrently measured in the literature, as displayed in Figure 2(B). Such unknown relationships were indirectly extracted from the combination of known relationships (Table 3) and typical ranges of values obtained from the literature for these properties. Due to the prior validation of the relationships in Table 6, these findings are reliable as indirectly consistent with the literature data processed in this study and provide new insights on the size-dependency of the MN recruitment mechanisms.

Extrapolation to rats and mice

It was assessed whether the scaled relationships obtained from cat data and reported in Table 6 could be successfully applied to rat and mouse data. A global $\{I_{th}; R\}$ dataset was obtained from 5 eligible rat studies reported in Table 7, while four mice studies reported in Table 7 provided processable data for the pairs $\{I_{th}; R\}$, $\{\tau; R\}$ and $\{C; R\}$. Figure 7 reports the global datasets for all 4 pairs of properties and the predictions obtained with the cat relationships reported in Table 6. As displayed in Table 7, r^2_{pred} and r^2_{exp}values were close for all 4 datasets, with a maximum 12.5% difference for $\{\tau; R\}$ in mice. $nRMSE$ values remained low in both rat and mouse $\{I_{th}; R\}$ datasets, while being substantially higher in both $\{\tau; R\}$ and $\{C; R\}$ datasets in mice because of an inter-species-specific offset in the relationships.

Table 7. Validation of the cat relationships (Table 6) against rat and mouse data. nME: normalized maximum error. nRMSE: normalized root-mean-square error. r^2_{pred}: coefficient of determination between experimental and predicted quantities. r^2_{exp} : coefficient of determination of the power trendline directly fitted to the experimental data.

Animal	Dataset	Reference studies	$\boldsymbol{nME}$ (%)	$\boldsymbol{nRMSE}$ (%)	$\boldsymbol{r^2_{pred}}$	$\boldsymbol{r^2_{exp}}$
Rat	$\{I_{th}; R\}$	(Gardiner, 1993; Bakels & Kernell, 1993; Lee & Heckman, 1998; Button et al., 2008; Turkin et al., 2010; Krutki et al., 2015)	591	16	0.53	0.54
Mouse	$\{I_{th}; R\}$	(Delestrée et al., 2014; De Lourdes Martínez-Silva et al., 2018; Huh et al., 2021)	621	17	0.37	0.41
	$\{\tau; R\}$	(Manuel et al., 2009b)	1183	155	0.35	0.40
	$\{C; R\}$	(Manuel et al., 2009b)	1802	87	0.38	0.38

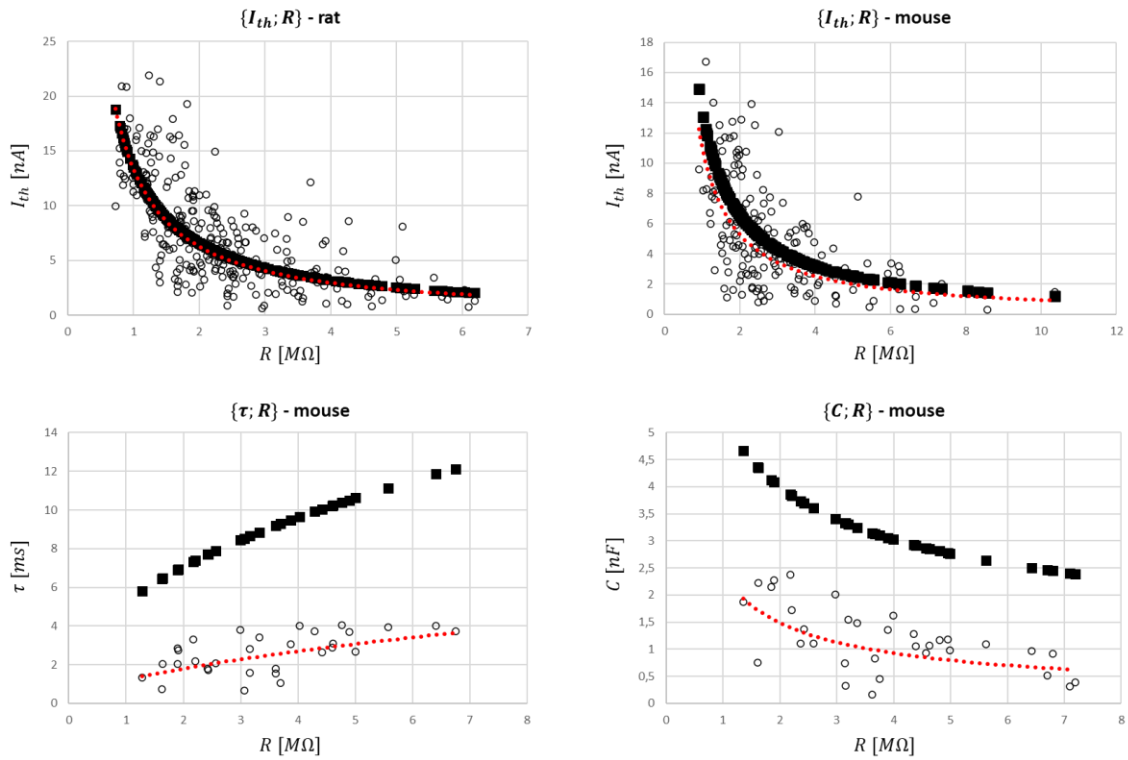

Figure 7. Global datasets for rat and mouse species and predictions of the MN properties with the cat mathematical relationships (Table 6). They were obtained from the 5 eligible studies on rats and the 4 eligible studies on mice reported in Table 7 that measured the $\{I_{th}; R\}$, $\{\tau; R\}$ and $\{C; R\}$ pairs of MN electrophysiological properties. I_{th}, R, τ, C are given in $nA, M\Omega, ms$ and nF respectively. The experimental data (○ symbol) is fitted with a power trendline (red dotted curve) and compared to the predicted quantities obtained with the scaled cat relationships in Table 6 (■ symbol).

Relationships between MN and mU properties

As shown in Figure 2(A), eight pairs of one MN and one mU property were investigated in 14 studies in the literature in cats and rats. As remarked by Heckman & Enoka (2012) and Manuel et al. (2019), most recent studies were performed on mice, while most dated were dominantly performed on cats. One study on the rat gastrocnemius muscle (Kanda & Hashizume, 1992) indicated no correlation between IR and CV. However, after removing from the dataset 2 outliers that fell outside two standard deviations of the mean IR data, a statistically significant correlation ($p < 0.05$) between IR and CV was successfully fitted with a power trendline ($r^2 = 0.43$). Eight studies, dominantly focusing on the cat soleus and medial gastrocnemius muscles, found a strong correlation between F^{tet} and CV, while one study showed a significant correlation for the pair $\{F^{tet}; R\}$ in both the cat tibialis anterior and extensor digitorum longus muscles. One study (Burke *et al.*, 1982) on the cat soleus, medial and lateral gastrocnemius muscles inferred a statistically significant correlation for $\{F^{tet}; S_{MN}\}$. In mice, both R and I_{th} were significantly related to muscle tetanic and twitch forces. As F^{tet}, F^{tw} and IR are

reliable indices of S_{mU} as discussed in the Methods, the MN size-dependent relationships in Table 3 return eight $S_{mU} = k \cdot S_{MN}^{c}$ relationships between mU and MN properties (Table 8). A 2.8-fold range in positive c-values $c \in [2.4; 6.6]$ (mean 3.8 ± 1.5 s.d.) was obtained between studies. This result infers than mU and MN size are positively related in cats, mice and potentially in rats.

Table 8. Fitted experimental data of pairs of one mU and one MN property and subsequent $\boldsymbol{S_{mU} \propto S_{MN}^{c}}$ relationships. The r^2, p-value and the equation $A \propto B^c$ of the trendlines are reported for each pair of properties. In the last column, prior knowledge is used to derive $S_{mU} \propto S_{MN}^{c}$ relationships.

Species	$\boldsymbol{A = k \cdot B^c}$ (fitted relationships)					$\boldsymbol{S_{mU} = k \cdot S_{MN}^{c}}$ (final relationships)
	Relationship	c	r^2	p-value	Reference studies	c
Rat	$IR = k \cdot CV^c$	3.4	0.45	$6 \cdot 10^{-3}$	(Kanda & Hashizume, 1992)	2.4
Cat	$F^{tw} = k \cdot CV^c$	9.4	0.43	$p < 10^{-5}$	(Knott et al., 1971)	6.6
	$F^{tet} = k \cdot CV^c$	7.2	0.37	$p < 10^{-5}$	(McPhedran et al., 1965; Wuerker et al., 1965; Appelberg & Emonet-Dénand, 1967; Proske & Waite, 1974; Bagust, 1974; Jami & Petit, 1975; Stephens & Stuart, 1975; Burke et al., 1982; Emonet-Dénand et al., 1988)	5.0
	$F^{tet} = k \cdot R^c$	-1.3	0.27	$6 \cdot 10^{-5}$	(Dum & Kennedy, 1980)	3.2
	$F^{tet} = k \cdot S_{MN}^{c}$	2.0	0.21	$2 \cdot 10^{-2}$	(Burke *et al.*, 1982)	2.0
Mouse	$F^{tw} = k \cdot R^c$	-2.1	0.42	$p < 10^{-5}$	(Manuel & Heckman, 2011; De Lourdes Martínez-Silva et al., 2018)	5.1
	$F^{tw} = k \cdot I_{th}^{c}$	1.3	0.64	$2 \cdot 10^{-4}$	(Manuel & Heckman, 2011)	3.3
	$F^{tet} = k \cdot I_{th}^{c}$	1.0	0.80	$6 \cdot 10^{-2}$	(Manuel & Heckman, 2011)	2.5
Mean $\pm$sd						3.8 ± 1.5

Discussion

In this systematic meta-analysis, we processed the data (Figure 3) from previous cat experimental studies to extract mathematical relationships between several MN electrophysiological properties and MN size. First, this allowed us to demonstrate that all investigated MN properties are predicted by MN size (Table 3, Figure 4, Figure 5) and that electrophysiological properties at the level of individual MNs are interrelated. Second, we established (Table 6) and validated (Figure 6) mathematical relationships linking all the pairs of MN properties, providing the first mathematical framework for building virtual MN pools of MN-specific morphometric and electrophysiological properties that are consistent with published experimental cat data *in vivo*.

The findings are consistent with considerations from previous literature reviews, either drawn from direct but isolated measurements or speculated. For example, Binder et al. (1996) concluded that the AHP duration was inversely related to MN size S_{MN} based on measures of a single experimental study. Conversely, the size-dependencies of R and I_{th} were qualitatively assumed by Powers & Binder (2001) from the equations obtained from a variant of Rall's model of MN membrane equivalent electrical circuit (Rall, 1957; Rall, 1959; Rall, 1960), and not from experimental data. The negative correlation between S_{MN} and R was predicted by Binder et al. (1996) from the findings of Henneman's studies on the correlation between extracellular spike amplitude and S_{MN} (Henneman, 1957; Henneman et al., 1965a). The fact that R defines the MN rheobase and thus dictates the size order of MN recruitment was similarly justified in Binder et al. (1996) and Powers & Binder (2001) from a combination of Henneman's findings and Rall's model equations. Moreover, all previous papers used the debated association between motor unit type and S_{MN} , mainly obtained from measures in the cat gastrocnemius muscle (Fleshman et al., 1981; Burke et al., 1982; Zengel et al., 1985; Bakels & Kernell, 1993), to indirectly speculate on correlations between S_{MN} and AHP (Heckman & Enoka, 2012), R (Powers & Binder, 2001; Heckman & Enoka, 2012), R_m (Binder et al., 1996; Powers & Binder, 2001) or I_{th} (Binder et al., 1996). Finally, we found a single paper that inferred a positive correlation between S_{MN} and C (Heckman & Enoka, 2012) but without reference to direct experimental results.

Relevance for MN modelling

The empirical equations in Table 6 provide a mathematical framework that supports the common approach of modelling the MN membrane behaviour with an equivalent resistance-capacitance electrical circuit as variants of Rall's cable model (Rall, 1957; Rall, 1959; Rall, 1960). The relationship $C = 1.0 \cdot 10^{-2} \cdot S_{MN}^{1.0}$ reported in Table 6 validates the definition $C = C_m \cdot S_{MN}$, as well as emphasizing that the specific capacitance C_m per unit area is constant among the MN pool, and indirectly yields, from typical ranges of C and S_{MN} in the literature, the relation $C_m = 1.0 \cdot 10^{-2} F \cdot m^{-2}$, which is highly

consistent with the typical values reported in the literature (Lux & Pollen, 1966; Albuquerque & Thesleff, 1968; Barrett & Crill, 1974; Adrian & Hodgkin, 1975; Sukhorukov et al., 1993; Major et al., 1994; Solsona et al., 1998; Thurbon et al., 1998; Gentet et al., 2000). Similarly, the empirical relationship $I_{th} = \frac{2.7 \cdot 10^{-2}}{R^{1.0}}$ (Table 6) yields $\Delta V_{th} = 27mV$, consistently with typical reported values (Brock et al., 1952; Eccles et al., 1958), despite uncertainties in the value of the membrane resting potential (Heckman & Enoka, 2012). This supports the conclusions that the relative voltage threshold ΔV_{th} is constant within the MN pool (Coombs et al., 1955; Gustafsson & Pinter, 1984a; Gustafsson & Pinter, 1984b; Powers & Binder, 2001), and that Ohm's law is followed in MNs (Glenn & Dement, 1981; Spruston & Johnston, 1992; Kernell, 2006). Also, no correlation between $\frac{\Delta V_{th}}{R \cdot I_{th}}$ and C is reported in Table 6, consistent with measurements performed by Gustafsson & Pinter (1984b), substantiating that the dynamics of MN recruitment dominantly rely on R, I^{th} and ΔV_{th} (Heckman & Enoka, 2012). Finally, the findings $R = 7.1 \cdot 10^{9} \cdot \tau^{1.6}, C = 1.6 \cdot 10^{-10} \cdot \frac{1}{\tau^{0.6}}$ and $R_m = 6.0 \cdot 10^{1} \cdot \tau$, $C_m = 1.0 \cdot 10^{-2} F \cdot m^{-2}$ in Table 6 yield $R \cdot C = 1.1 \cdot \tau$ and $R_m \cdot C_m = 0.6 \cdot \tau$, which is consistent with the classic empirical relationship $\tau = RC = R_m C_m$ (Gustafsson & Pinter, 1984a; Zengel et al., 1985).

Relevance for other mammals

It is demonstrated in Figure 7 and with the calculation of the r^2 values in Table 7 that the mathematical equations in Table 6 obtained from cat data adequately predict the normalized associations between pairs of MN properties in rats and mice. However, the scaling factor K applied to the intercept k_e to scale the normalized relationships $A = K \cdot k_e \cdot B^e$ is species-specific, being for example around 3 times less in mice than in cat for the $\{\tau; R\}$ and $\{C; R\}$ pairs in mice (Figure 7) and explaining the large obtained $nRMSE$ values in these cases. Absolute values of the $\{I_{th}; R\}$ pair were nevertheless accurately predicted in both rats and mice from the cat relationships, as explained by the larger values of R which counterbalances the respectively lower I_{th} values in mice and rats than in cats (Manuel et al., 2019; Highlander et al., 2020). Therefore, the mathematical equations in Table 6 should be used for the modelling of cat MN pools only, while the normalized equations in Supplementary material should be used and scaled with species-specific data if investigating other mammals (mice, rats, humans). It was not assessed whether these relationships applied to non-mammal species.

Henneman's size principle of motor unit (MU) recruitment

Table 8 reports statistically significant power relationships of positive power values between MN and mU indices of size. These results substantiate the concept that S_{MN} and S_{mU} are positively correlated in a MU pool and that large MNs innervate large mUs (Henneman, 1981; Heckman & Enoka, 2012), a statement that has never been demonstrated from the concurrent direct measurement of S_{MN} and

652 S_{mU}. Besides, considering the positive $I_{th} - S_{MN}$ correlation (Table 6), and that the mU force
653 recruitment threshold F^{th} is positively correlated to F^{tet} (Heckman & Enoka, 2012) and thus to S_{mU}
654 (Table 2), larger MUs have both larger current and force recruitment thresholds I_{th} and F^{th} than
655 relatively smaller MUs, which are thus recruited first, consistently with the Henneman's size principle
656 of MU recruitment (Henneman, 1957; Wuerker et al., 1965; Henneman et al., 1965a; Henneman et al.,
657 1965b; Henneman et al., 1974; Henneman, 1981; Henneman, 1985). The terminologies 'small MU',
658 'low-force MU' and 'low-threshold MU' are thus equivalent. Henneman's size principle thus relies on
659 the amplitude of the MN membrane resistance (Binder et al., 1996; Powers & Binder, 2001; Heckman
660 & Enoka, 2012). Finally, the relationships $S_{MN} \propto CV^{1.4} \propto \tau^{-0.7} \propto AHP^{-0.7}$ (Table 6) suggest that high-
661 threshold MUs rely on relatively faster MN dynamics, which might partially explain why large MNs can
662 attain relatively larger firing rates than low-thresholds MNs.

663 It has been repeatedly attempted to extend Henneman's size principle and the correlations between
664 the MU properties in Table 1 to the concept of 'MU type' (Burke & Ten Bruggencate, 1971; Burke,
665 1981; Bakels & Kernell, 1993; Powers & Binder, 2001). While a significant association between 'MU
666 type' and indices of MU size has been observed in some animal (Fleshman et al., 1981; Burke et al.,
667 1982; Zengel et al., 1985) and a few human (Milner-Brown et al., 1973; Stephens & Usherwood, 1977;
668 Garnett et al., 1979; Andreassen & Arendt-Nielsen, 1987) studies, it has however not been observed
669 in other animal studies ((Bigland-Ritchie et al., 1998) for a review) and in the majority of human
670 investigations (Sica & McComas, 1971; Goldberg & Derfler, 1977; Yemm, 1977; Young & Mayer, 1982;
671 Thomas et al., 1990; Nordstrom & Miles, 1990; Elek et al., 1992; Macefield et al., 1996; Cutsem et al.,
672 1997; Mateika et al., 1998; Fuglevand et al., 1999; Keen & Fuglevand, 2004). Moreover, the reliability
673 of these results is weakened by the strong limitations of the typical MU type identification protocols.
674 Sag experiments are irrelevant in humans (Buchthal & Schmalbruch, 1970; Thomas et al., 1991; Bakels
675 & Kernell, 1993; Macefield et al., 1996; Bigland-Ritchie et al., 1998; Fuglevand et al., 1999), and lack
676 consistency with other identification methods (Nordstrom & Miles, 1990). MU type identification by
677 twitch contraction time measurements is limited by the strong sources of inaccuracy involved in the
678 transcutaneous stimulation, intramuscular microstimulation, intraneural stimulation, and spike-
679 triggered averaging techniques (Taylor et al., 2002; Keen & Fuglevand, 2004; McNulty & Macefield,
680 2005; Negro et al., 2014; Dideriksen & Negro, 2018). Finally, as muscle fibres show a continuous
681 distribution of contractile properties among the MU pool, some MUs fail to be categorized in discrete
682 MU types in some animal studies by histochemical approaches (Reinking et al., 1975; Totosy de
683 Zepetnek et al., 1992). Owing to these conflicting results and technical limitations, MU type may not
684 be related to MN size and the basis for MU recruitment during voluntary contractions (McNulty &
685 Macefield, 2005; Duchateau & Enoka, 2011).

686 **Limitations**

687 The mathematical relationships derived Table 6 and the conclusions drawn in the Discussion present
688 some limitations, which were partly discussed in the Methods and Result sections and are summarised
689 here. A first limitation is related to the normalization of all datasets to the highest measured value
690 retrieved in each study; this approach is only valid if the experimental studies identified the same
691 largest MN relatively to the MN populations under investigation. This cannot be verified and is unlikely
692 considering the small MN populations investigated in most eligible studies. A second limitation is due
693 to the limited processable experimental data available in the literature, especially in rats and mice, as
694 also discussed by Heckman & Enoka (2012). Therefore, some pairs of MN properties were investigated
695 in only one study, especially those involving C, preventing inter-study comparisons. Also for this
696 reason, measurements obtained from MNs innervating different muscles from cats of different sex
697 were merged into unique datasets, implicitly assuming no sex- and muscle-specific distributions of MN
698 properties within the MN pools. Besides, only MNs innervating the hindlimbs were investigated. The
699 extrapolation of the relationships in Table 6 to rat and mouse species could only be assessed against a
700 small set of studies and for three associations only. Finally, the conclusions on the associations
701 between S_{mU} and S_{MN} relied on few studies providing few measurements, due to the challenging
702 experimental protocols and the considerable amount of work required to measure both MN and mU
703 properties in single MUs. Thirdly, the available data comes from relatively dated cat studies, as
704 observed in Manuel et al. (2019). Thus, recent computer-assisted techniques of MN morphometric
705 measurements were notably not applicable in those studies, yielding important sources of
706 inaccuracies, as discussed. Therefore, the relationships involving S_{neuron} are subjected to a higher
707 level of inaccuracy. Consequently, the mathematical relationships in Table 6 best reproduce published
708 cat data but might remain a crude description of the association of MN properties in real MN pools.
709 They however meet the level of inaccuracy that would be obtained from direct experimental
710 approaches.

711 **Conclusion**

712 This study provides the first empirical and algebraical proof that the MN size S_{MN} and the MN
713 electrophysiological properties (ACV, AHP, R, I_{th}, C and τ) are related. The derived mathematical
714 relationships between any of these MN properties and/or S_{MN} are provided in Table 6. They accurately
715 describe the experimental cat data available in the literature and provide for the first time a method
716 for building virtual MN profiles of inter-consistent MN-specific properties in mammals and a
717 framework to generate hypothesis for experimental studies aiming at investigating currently
718 unreported relationships.

References

Adrian RH, Hodgkin AL (1975) Conduction velocity and gating current in the squid giant axon. Proc. Royal Soc. 189:81-86.

Albuquerque EX, Thesleff S (1968) A comparative study of membrane properties of innervated and chronically denervated fast and slow skeletal muscles of the rat. Acta Physiol. Scand. 73:471-480.

Amendola J, Durand J (2008) Morphological differences between wild-type and transgenic superoxide dismutase 1 lumbar motoneurons in postnatal mice. Journal of comparative neurology (1911) 511:329-341.

Andreassen S, Arendt-Nielsen L (1987) Muscle fibre conduction velocity in motor units of the human anterior tibial muscle: A new size principle parameter. J. Physiol. 391:561-571.

Ankit, R. (2020) WebPlotDigitizer. **4.4** https://automeris.io/WebPlotDigitizer.

Appelberg B, Emonet-Dénand F (1967) Motor units of the first superficial lumbrical muscle of the cat. J. Neurophysiol. 30:154-160.

Bagust J (1974) Relationships between motor nerve conduction velocities and motor unit contraction characteristics in a slow twitch muscle of the cat. J. Physiol. 238:269-278.

Bakels R, Kernell D (1993) Matching between motoneurone and muscle unit properties in rat medial gastrocnemius. J. Physiol. 463:307-324.

Barrett JN, Crill WE (1974) Specific membrane properties of cat motoneurones. J. Physiol. 239:301-324.

Bigland-Ritchie B, Fuglevand AJ, Thomas CK (1998) Contractile properties of human motor units: Is man a cat? The Neuroscientist 4:240-249.

Binder, M. D., Heckman, C. J. & Powers, R. K. (1996) The physiological control of motoneuron activity. In Rowell LB, S. J. (ed), *Handbook of Physiology: Exercise, Regulation and Integration of Multiple Systems.* New York: Oxford Univ Press, pp. 3-53.

Bodine SC, Roy RR, Eldred E, Edgerton VR (1987) Maximal force as a function of anatomical features of motor units in the cat tibialis anterior. J. Neurophysiol. 57:1730-1745.

Brandenburg, J. E.,Fogarty, M.J.,Brown, A.D.,Sieck, G.C.(2020) Phrenic motor neuron loss in an animal model of early onset hypertonia. Journal of Neurophysiology, **123**, 1682.

Brandenburg, J. E.,Gransee, H.M.,Fogarty, M.J.,Sieck, G.C.(2018) Differences in lumbar motor neuron pruning in an animal model of early onset spasticity. Journal of Neurophysiology, **120**, 601.

Brock LG, Coombs JS, Eccles JC (1952) The recording of potentials from motoneurones with an intracellular electrode. J.Physiol.(Lond.) 117:431-460.

Buchthal F, Schmalbruch H (1970) Contraction times and fibre types in intact human muscle. Acta Physiol. Scand. 79:435-452.

Burke RE, Ten Bruggencate G (1971) Electrotonic characteristics of alpha motoneurones of varying size. J. Physiol. 212:1-20.

Burke RE, Dum RP, Fleshman JW, Glenn LL, Lev-Tov A, O'Donovan MJ, Pinter MJ (1982) An HRP study of the relation between cell size and motor unit type in cat ankle extensor motoneurons. J. Comp. Neurol. 209:17-28.

Burke RE, Tsairis P (1973) Anatomy and innervation ratios in motor units of cat gastrocnemius. J. Physiol. 234:749-765.

Burke RE (1968) Firing patterns of gastrocnemius motor units in the decerebrate cat. J. Physiol. 196:631-654.

Burke, R. E. (1981) Motor units: Anatomy, physiology, and functional organization. In Brooks, V. B. (ed), *Handbook of Physiology, the Nervous System, Motor Control.* American Physiological Society, pp. 345-422.

Button DC, Kalmar JM, Gardiner K, Marqueste T, Zhong H, Roy RR, Edgerton VR, Gardiner PF (2008) Does elimination of afferent input modify the changes in rat motoneurone properties that occur following chronic spinal cord transection? The Journal of physiology 586:529-544.

Carp JS, Tennissen AM, Mongeluzi DL, Dudek CJ, Chen XY, Wolpaw JR (2008) An in vitro protocol for recording from spinal motoneurons of adult rats. Journal of Neurophysiology 100:474-481.

Carrascal L, Nieto-Gonzalez JL, Torres B, Nunez-Abades P (2009) Changes in somatodendritic morphometry of rat oculomotor nucleus motoneurons during postnatal development. Journal of comparative neurology (1911) 514:189-202.

Chamberlain S, Lewis DM (1989) Contractile characteristics and innervation ratio of rat soleus motor units. J. Physiol. 412:1-21.

Coombs JS, Eccles JC, Fatt P (1955) The electrical properties of the motoneurone membrane. J.Physiol.(Lond.) 130:291-325.

Copray, S.,Kernell, D.(2000) Neurotrophins and trk-receptors in adult rat spinal motoneurons: Differences related to cell size but not to ‘slow/fast’ specialization. Neuroscience Letters, **289**, 217.

Cullheim S, Fleshman JW, Glenn LL, Burke RE (1987) Membrane area and dendritic structure in type-identified triceps surae alpha motoneurons. Journal of comparative neurology (1911) 255:68-81.

Cullheim S (1978) Relations between cell body size, axon diameter and axon conduction velocity of cat sciatic α-motoneurons stained with horseradish peroxidase. Neurosci. Lett. 8:17-20.

Cutsem MV, Feiereisen P, Duchateau J, Hainaut K (1997) Mechanical properties and behaviour of motor units in the tibialis anterior during voluntary contractions. Can. J. Appl. Physiol. 22:585-597.

De Lourdes Martínez-Silva M, Imhoff-Manuel RD, Sharma A, Heckman CJ, Shneider NA, Roselli F, Zytnicki D, Manuel M (2018) Hypoexcitability precedes denervation in the large fast-contracting motor units in two unrelated mouse models of ALS. ELife 7:e30955.

788 Deardorff AS, Romer SH, Deng Z, Bullinger KL, Nardelli P, Cope TC, Fyffe REW (2013) Expression of
789 postsynaptic Ca2+-activated K+ (SK) channels at C-bouton synapses in mammalian lumbar -
790 motoneurons. The Journal of physiology 591:875-897.

791 Delestrée, N.,Manuel, M.,Iglesias, C.,Elbasiouny, S.M.,Heckman, C.J.,Zytnicki, D.(2014) Adult spinal
792 motoneurones are not hyperexcitable in a mouse model of inherited amyotrophic lateral sclerosis.
793 The Journal of Physiology, **592**, 1687.

794 Destombes J, Horcholle-Bossavit G, Thiesson D, Jami L (1992) Alpha and gamma motoneurons in the
795 peroneal nuclei of the cat spinal cord: An ultrastructural study. Journal of comparative neurology
796 (1911) 317:79-90.

797 Dideriksen JL, Negro F (2018) Spike-triggered averaging provides inaccurate estimates of motor unit
798 twitch properties under optimal conditions. J Electromyogr Kinesiol 43:104-110.

799 Dong Y, Mihalas S, Russell A, Etienne-Cummings R, Niebur E (2011) Estimating parameters of
800 generalized integrate-and-fire neurons from the maximum likelihood of spike trains. Neural Comput.
801 23:2833-2867.

802 Donselaar Y, Kernell D, Eerbeek O (1986) Soma size and oxidative enzyme activity in normal and
803 chronically stimulated motoneurones of the cat's spinal cord. Brain Research 385:.

804 Duchateau J, Enoka RM (2011) Human motor unit recordings: Origins and insight into the integrated
805 motor system. Brain Res. 1409:42-61.

806 Dukkipati, S. S.,Garrett, T.L.,Elbasiouny, S.M.(2018) The vulnerability of spinal motoneurons and
807 soma size plasticity in a mouse model of amyotrophic lateral sclerosis. J Physiol, **596**, 1723.

808 Dum RP, Kennedy TT (1980) Physiological and histochemical characteristics of motor units in cat
809 tibialis anterior and extensor digitorum longus muscles. J. Neurophysiol. 43:1615-1630.

810 Eccles JC, Libet B, Young RR (1958) The behaviour of chromatolysed motoneurones studied by
811 intracellular recording. J.Physiol.(Lond.) 143:11-40.

812 Eccles JC, Eccles RM, Lundberg A (1957) Durations of after-hyperpolarization of motoneurones
813 supplying fast and slow muscles. Nature 179:866-868.

814 Elek JM, Kossev A, Dengler R, Schubert M, Wohlfahrt K, Wolf W (1992) Parameters of human motor
815 unit twitches obtained by intramuscular microstimulation. Neuromuscul. Disord. 2:261-267.

816 Emonet-Dénand F, Hunt CC, Petit J, Pollin B (1988) Proportion of fatigue-resistant motor units in
817 hindlimb muscles of cat and their relation to axonal conduction velocity. J. Physiol. 400:135-158.

818 Enoka RM (1995) Morphological features and activation patterns of motor units. J Clin Neurophysiol
819 12:538-559.

820 Filipchuk AA, Durand J (2012) Postnatal dendritic development in lumbar motoneurons in mutant
821 superoxide dismutase 1 mouse model of amyotrophic lateral sclerosis. Neuroscience 209:144-154.

822 Fleshman JW, Munson JB, Sypert GW, Friedman WA (1981) Rheobase, input resistance, and motor-
823 unit type in medial gastrocnemius motoneurons in the cat. J Neurophysiol 46:1326-1338.

824 Foehring RC, Sypert GW, Munson JB (1987) Motor-unit properties following cross-reinnervation of
825 cat lateral gastrocnemius and soleus muscles with medial gastrocnemius nerve. II. influence of
826 muscle on motoneurons. J Neurophysiol 57:1227-1245.

827 Foehring RC, Sypert GW, Munson JB (1986) Properties of self-reinnervated motor units of medial
828 gastrocnemius of cat. II. axotomized motoneurons and time course of recovery. J Neurophysiol
829 55:947-965.

830 Fogarty, M. J.,Mu, E.W.H.,Lavidis, N.A.,Noakes, P.G.,Bellingham, M.C.(2020) Size-Dependent
831 vulnerability of lumbar motor neuron dendritic degeneration in SOD1 G93A mice. Anat. Rec., **303**,
832 1455.

833 Fogarty MJ, Omar TS, Zhan W, Mantilla CB, Sieck GC (2018) Phrenic motor neuron loss in aged rats.
834 J.Neurophysiol. 119:1852-1862.

835 Frank K, Fuortes M (1956) Stimulation of spinal motoneurones with intracellular electrodes.
836 J.Physiol.(Lond.) 134:451-470.

837 Friese A, Kaltschmidt JA, Ladle DR, Sigrist M, Jessell TM, Arber S (2009) Gamma and alpha motor
838 neurons distinguished by expression of transcription factor Err3. Proceedings of the National
839 Academy of Sciences - PNAS 106:13588-13593.

840 Fuglevand AJ, Macefield VG, Bigland-Ritchie B (1999) Force-frequency and fatigue properties of
841 motor units in muscles that control digits of the human hand. J Neurophysiol 81:1718-1729.

842 Gao H, Glatzer NR, Williams KW, Derbenev AV, Liu D, Smith BN (2009) Morphological and
843 electrophysiological features of motor neurons and putative interneurons in the dorsal vagal
844 complex of rats and mice. Brain research 1291:40-52.

845 Gardiner PF (1993) Physiological properties of motoneurons innervating different muscle unit types
846 in rat gastrocnemius. J Neurophysiol 69:1160-1170.

847 Garnett RAF, O'Donovan MJ, Stephens JA, Taylor A (1979) Motor unit organization of human medial
848 gastrocnemius. J. Physiol. 287:33-43.

849 Gentet L, Stuart GJ, Clements JD (2000) Direct measurement of specific membrane capacitance in
850 neurons. Biophys. J. 79:314-320.

851 Glenn LL, Dement WC (1981) Membrane resistance and rheobase of hindlimb motoneurons during
852 wakefulness and sleep. J Neurophysiol 46:1076-1088.

853 Goldberg LJ, Derfler B (1977) Relationship among recruitment order, spike amplitude, and twitch
854 tension of single motor units in human masseter muscle. J Neurophysiol 40:879-890.

855 Gustafsson, Pinter MJ (1985) On factors determining orderly recruitment of motor units: A role for
856 intrinsic membrane properties. Trends Neurosci. 431-433.

857 Gustafsson, Pinter MJ (1984a) Relations among passive electrical properties of lumbar alpha-
858 motoneurones of the cat. J. Physiol. 356:401-431.

Gustafsson, Pinter MJ (1984b) An investigation of threshold properties among cat spinal alpha-motoneurones. J. Physiol. 357:453-483.

Gustafsson B (1979) Changes in motoneurone electrical properties following axotomy. J. Physiol. 293:197-215.

Heckman CJ, Enoka RM (2012) Motor unit. Compr. Physiol. 2:2629-2682.

Hegedus J, Putman CT, Gordon T (2007) Time course of preferential motor unit loss in the SOD1 G93A mouse model of amyotrophic lateral sclerosis. Neurobiology of disease 28:154-164.

Henneman E (1985) The size-principle: A deterministic output emerges from a set of probabilistic connections. J. Exp. Biol. 115:105-112.

Henneman E (1981) Recruitment of motoneurons : The size principle. Motor Unit Types, Recruitment and Plasticity in Health and Disease 26-60.

Henneman E, Clamann HP, Gillies JD, Skinner RD (1974) Rank order of motoneurons within a pool: Law of combination. J Neurophysiol 37:1338-1349.

Henneman E, Somjen G, Carpenter DO (1965a) Functional significance of cell size in spinal motoneurons. J Neurophysiol 28:560-580.

Henneman E, Somjen G, Carpenter DO (1965b) Excitability and inhibitibility of motoneurons of different sizes. J Neurophysiol 28:599-620.

Henneman E (1957) Relation between size of neurons and their susceptibility to discharge. Science 126:1345-1347.

Highlander, M. M.,Allen, J.M.,Elbasiouny, S.M.(2020) Meta-analysis of biological variables' impact on spinal motoneuron electrophysiology data. Journal of Neurophysiology, **123**, 1380.

Huh, S.,Heckman, C.J.,Manuel, M.(2021) Time course of alterations in adult spinal motoneuron properties in the SOD1(G93A) mouse model of ALS. eNeuro, **8**, ENEURO.

Ishihara, A.,Kawano, F.,Ishioka, N.,Oishi, H.,Higashibata, A.,Shimazu, T.,Ohira, Y.(2001) Growth-related changes in cell body size and succinate dehydrogenase activity of spinal motoneurons innervating the rat soleus muscle. Int. j. dev. neurosci., **21**, 461.

Issa AN, Zhan W, Sieck GC, Mantilla CB (2010) Neuregulin-1 at synapses on phrenic motoneurons. J.Comp.Neurol. 518:4213-4225.

Izhikevich EM (2004) Which model to use for cortical spiking neurons? IEEE Trans.Neural Networks 15:1063-1070.

Jami L, Petit J (1975) Correlation between axonal conduction velocity and tetanic tension of motor units in four muscles of the cat hind limb. Brain Res. 96:114-118.

Kanda K, Hashizume K (1992) Factors causing difference in force output among motor units in the rat medial gastrocnemius muscle. J. Physiol. 448:677-695.

Kanjhan, R.,Fogarty, M.J.,Noakes, P.G.,Bellingham, M.C.(2015) Developmental changes in the morphology of mouse hypoglossal motor neurons. Brain Struct Funct, **221**, 3755.

Keen DA, Fuglevand AJ (2004) Distribution of motor unit force in human extensor digitorum assessed by spike-triggered averaging and intraneural microstimulation. J Neurophysiol 91:2515-2523.

Kernell D (2006) *The Motoneurone and its Muscle Fibres.* Oxford University Press UK, .

Kernell D, Zwaagstra B (1989) Dendrites of cat's spinal motoneurones: Relationship between stem diameter and predicted input conductance. J. Physiol. 413:255-269.

Kernell D, Monster AW (1981) Threshold current for repetitive impulse firing in motoneurones innervating muscle fibres of different fatigue sensitivity in the cat. Brain Res. 229:193-196.

Kernell D, Zwaagstra B (1981) Input conductance, axonal conduction velocity and cell size among hindlimb motoneurones of the cat. Brain Res. 204:311-326.

Kernell D (1966) Input resistance, electrical excitability, and size of ventral horn cells in cat spinal cord. Science 152:1637-1640.

Knott S, Lewis DM, Luck JC (1971) Motor unit areas in a cat limb muscle. Exp.Neurol. 30:475-483.

Krawitz S, Fedirchuk B, Dai Y, Jordan LM, McCrea DA (2001) State-dependent hyperpolarization of voltage threshold enhances motoneurone excitability during fictive locomotion in the cat. The Journal of physiology 532:271-281.

Krutki P, Hałuszka A, Mrówczyński W, Gardiner PF, Celichowski J (2015) Adaptations of motoneuron properties to chronic compensatory muscle overload. Journal of neurophysiology 113:2769-2777.

Lee RH, Heckman CJ (1998) Bistability in spinal motoneurons in vivo: Systematic variations in persistent inward currents. Journal of neurophysiology 80:583-593.

Li Y, Brewer D, Burke RE, Ascoli GA (2005) Developmental changes in spinal motoneuron dendrites in neonatal mice. Journal of comparative neurology (1911) 483:304-317.

Lucas SM, Ruff RL, Binder MD (1987) Specific tension measurements in single soleus and medial gastrocnemius muscle fibers of the cat. Exp.Neurol. 95:142-154.

Lux HD, Pollen DA (1966) Electrical constants of neurons in the motor cortex of the cat. J.Neurophysiol. 29:207-220.

Macefield VG, Fuglevand AJ, Bigland-Ritchie B (1996) Contractile properties of single motor units in human toe extensors assessed by intraneural motor axon stimulation. J Neurophysiol 75:2509-2519.

Major G, Larkman AU, Jonas P, Sakmann B, Jack JJ (1994) Detailed passive cable models of whole-cell recorded CA3 pyramidal neurons in rat hippocampal slices. J.Neurosci. 14:4613-4638.

Mantilla, C. B.,Zhan, W.,Gransee, H.M.,Prakash, Y.S.,Sieck, G.C.(2018) Phrenic motoneuron structural plasticity across models of diaphragm muscle paralysis. J Comp Neurol, **526**, 2973.

Manuel M, Chardon M, Tysseling V, Heckman CJ (2019) Scaling of motor output, from mouse to humans. Physiology (Bethesda, Md.) 34:5-13.

Manuel M, Heckman CJ (2011) Adult mouse motor units develop almost all of their force in the subprimary range: A new all-or-none strategy for force recruitment? Journal of Neuroscience 31:15188-15194.

Manuel M, Iglesias C, Donnet M, Leroy F, Heckman CJ, Zytnicki D (2009a) Fast kinetics, high-frequency oscillations, and subprimary firing range in adult mouse spinal motoneurons. The Journal of neuroscience 29:11246-11256.

Manuel M, Iglesias C, Donnet M, Leroy F, Heckman CJ, Zytnicki D (2009b) Fast kinetics, high-frequency oscillations, and subprimary firing range in adult mouse spinal motoneurons. The Journal of neuroscience 29:11246-11256.

Mateika JH, Essif EG, Dellorusso C, Fregosi RF (1998) Contractile properties of human nasal dilator motor units. J Neurophysiol 79:371-378.

McNulty PA, Macefield VG (2005) Intraneural microstimulation of motor axons in the study of human single motor units. Muscle & Nerve: Official Journal of the American Association of Electrodiagnostic Medicine 32:119-139.

McPhedran AM, Wuerker RB, Henneman E (1965) Properties of motor units in a homogeneous red muscle (soleus) of the cat. J Neurophysiol 28:71-84.

Mierzejewska-Krzyżowska B, Bukowska D, Taborowska M, Celichowski J (2014) Sex differences in the number and size of motoneurons innervating rat medial gastrocnemius muscle. Anatomia, histologia, embryologia 43:182-189.

Milner-Brown HS, Stein RB, Yemm R (1973) The orderly recruitment of human motor units during voluntary isometric contractions. J. Physiol. 230:359-370.

Mitra P, Brownstone RM (2012) An in vitro spinal cord slice preparation for recording from lumbar motoneurons of the adult mouse. Journal of Neurophysiology 107:728-741.

Moschovakis AK, Burke RE, Fyffe REW (1991) The size and dendritic structure of HRP-labeled gamma motoneurons in the cat spinal cord. Journal of comparative neurology (1911) 311:531-545.

Munson JB, Foehring RC, Lofton SA, Zengel JE, Sypert GW (1986) Plasticity of medial gastrocnemius motor units following cordotomy in the cat. Journal of neurophysiology 55:1454.

Nakanishi ST, Whelan PJ (2010) Diversification of intrinsic motoneuron electrical properties during normal development and botulinum Toxin–Induced muscle paralysis in early postnatal mice. J.Neurophysiol. 103:2833-2845.

Negro F, Yavuz U, Farina D (2016) The human motor neuron pools receive a dominant slow-varying common synaptic input. J. Physiol. 594:5491-5505.

Negro F, Yavuz U, Farina D (2014) Limitations of the spike-triggered averaging for estimating motor unit twitch force: A theoretical analysis. PloS one 9:e92390.

Nordstrom MA, Miles TS (1990) Fatigue of single motor units in human masseter. J. Appl. Physiol. 68:26-34.

Obregón G, Ermilov LG, Wen-Zhi Z, Sieck GC, Mantilla CB (2009) Modeling dendritic arborization based on 3D-reconstructions of adult rat phrenic motoneurons. Revista Ingeniería Biomédica 3:47-54.

Pinter MJ, Vanden Noven S (1989) Effects of preventing reinnervation on axotomized spinal motoneurons in the cat. I. motoneuron electrical properties. Journal of neurophysiology 62:311-324.

Powers RK, Binder MD (2001) Input-output functions of mammalian motoneurons. Rev. Physiol. Biochem. Pharmacol. 143:137-263.

Prakash YS, Mantilla CB, Zhan W, Smithson KG, Sieck GC (2000) Phrenic motoneuron morphology during rapid diaphragm muscle growth. Journal of Applied Physiology 89:563-572.

Proske U, Waite PME (1974) Properties of types of motor units in the medial gastrocnemius muscle of the cat. Brain Res. 67:89-101.

Rafuse VF, Pattullo MC, Gordon T (1997) Innervation ratio and motor unit force in large muscles: A study of chronically stimulated cat medial gastrocnemius. J. Physiol. 499:809-823.

Rall W (1960) Membrane potential transients and membrane time constant of motoneurons. Exp.Neurol. 2:503-532.

Rall W (1959) Branching dendritic trees and motoneuron membrane resistivity. Exp.Neurol. 1:491-527.

Rall W (1957) Membrane time constant of motoneurons. Science 126:454.

Reinking RM, Stephens JA, Stuart DG (1975) The motor units of cat medial gastrocnemius: Problem of their categorisation on the basis of mechanical properties. Exp. Brain Res. 23:301-313.

Sasaki M (1991) Membrane properties of external urethral and external anal sphincter motoneurones in the cat. The Journal of physiology 440:345-366.

Sica REP, McComas AJ (1971) Fast and slow twitch units in a human muscle. J. Neurol. Neurosurg. Psychiatry 34:113-120.

Solsona C, Innocenti B, Fernández JM (1998) Regulation of exocytotic fusion by cell inflation. Biophys.J. 74:1061-1073.

Song Z, Hu J, Rudy B, Redman SJ (2006) Developmental changes in the expression of calbindin and potassium-channel subunits Kv3. 1b and Kv3. 2 in mouse renshaw cells. Neuroscience 139:531-538.

Spruston N, Johnston D (1992) Perforated patch-clamp analysis of the passive membrane properties of three classes of hippocampal neurons. J Neurophysiol 67:508-529.

Stephens JA, Stuart DG (1975) The motor units of cat medial gastrocnemius: Speed-size relations and their significance for the recruitment order of motor units. Brain. Res. 91:177-195.

Stephens JA, Usherwood TP (1977) The mechanical properties of human motor units with special reference to their fatiguability and recruitment threshold. Brain Res. 125:91-97.

Sukhorukov VL, Arnold WM, Zimmermann U (1993) Hypotonically induced changes in the plasma membrane of cultured mammalian cells. J.Membr.Biol. 132:27-40.

Swett, Wikholm, Blanks, Conley (1986) Motoneurons of the rat sciatic nerve. Exp. Neurol. 93:227-252.

Taylor AM, Steege JW, Enoka RM (2002) Motor-unit synchronization alters spike-triggered average force in simulated contractions. J Neurophysiol 88:265-276.

Teeter C, Iyer R, Menon V, Gouwens N, Feng D, Berg J, Szafer A, Cain N, Zeng H, Hawrylycz M, Koch C, Mihalas S (2018) Generalized leaky integrate-and-fire models classify multiple neuron types. Nat Commun 9:1-15.

Thomas CK, Bigland-Richie B, Johansson RS (1991) Force-frequency relationships of human thenar motor units. J. Neurophysiol. 65:1509-1516.

Thomas CK, Johansson RS, Westling G, Bigland-Ritchie B (1990) Twitch properties of human thenar motor units measured in response to intraneural motor-axon stimulation. J Neurophysiol 64:1339-1346.

Thurbon D, Hans-R. Lüscher, Hofstetter T, Redman SJ (1998) Passive electrical properties of ventral horn neurons in rat spinal cord slices. J.Neurophysiol. 79:2485-2502.

Totosy de Zepetnek, Zung HV, Erdebil S, Gordon T (1992) Innervation ratio is an important determinant of force in normal and reinnervated rat tibialis anterior muscles. J Neurophysiol 67:1385-1403.

Turkin VV, O'Neill D, Jung R, Iarkov A, Hamm TM (2010) Characteristics and organization of discharge properties in rat hindlimb motoneurons. Journal of Neurophysiology 104:1549-1565.

Ulfhake, Kellerth JO (1981) A quantitative light microscopic study of the dendrites of cat spinal α-motoneurons after intracellular staining with horseradish peroxidase. J. Comp. Neurol. 202:571-583.

Ulfhake B, Kellerth JO (1984) Electrophysiological and morphological measurements in cat gastrocnemius and soleus α-motoneurones. Brain Res. 307:167-179.

Ulfhake B, Cullheim S (1988) Postnatal development of cat hind limb motoneurons. III: Changes in size of motoneurons supplying the triceps surae muscle. Journal of comparative neurology (1911) 278:103-120.

von Steyern FV, Martinov V, Rabben I, Njå A, de Lapeyrière O, Lømo T (1999) The homeodomain transcription factors islet 1 and HB9 are expressed in adult alpha and gamma motoneurons identified by selective retrograde tracing. The European journal of neuroscience 11:2093-2102.

Wuerker RB, McPhedran AM, Henneman E (1965) Properties of motor units in a heterogeneous pale muscle (m. gastrocnemius) of the cat. J.Neurophysiol. 28:85-99.

Yemm R (1977) The orderly recruitment of motor units of the masseter and temporal muscles during voluntary isometric contraction in man. J. Physiol. 265:163-174.

Young JL, Mayer RF (1982) Physiological alterations of motor units in hemiplegia. J. Neurol. Sci. 54:401-412.

Zengel JE, Reid SA, Sypert GW, Munson JB (1985) Membrane electrical properties and prediction of motor-unit type of medial gastrocnemius motoneurons in the cat. J Neurophysiol 53:1323-1344.

Zwaagstra, Kernell (1981) Sizes of soma and stem dendrites in intracellularly labelled α-motoneurones of the cat. Brain Research 204:295-309.

Zwaagstra B, Kernell D (1980) The duration of after-hyperpolarization in hindlimb alpha motoneurones of different sizes in the cat. Neurosci. Lett. 19:303-307.